Response to Review of "Extreme temperature and precipitation response to solar dimming and stratospheric aerosol geoengineering" by D. Ji et al.

We first thank the referee for his/her insightful comments, which helped us clarify and greatly improve the paper. In the reply, the referee's comments are in *italics*, our response is in normal and changes to the text are shown in blue.

Anonymous Referee #1

The authors analyze GeoMIP experiments G1 and G4 on extreme values. So far, this has only be done for G1 results (solar dimming) but not for injection of sulfate into the stratosphere. They try to estimate differences in the efficiency of the two models, despite the large differences in the forcing.
The paper is mostly well written. I recommend publication when the following after the authors addressed the following comments and questions.

General:
Some results in Figures 6, 7 and 8 are not clearly described and need further explanations. Also the amount of single figures within these figures can be reduced.

Reply: Thanks. We revise Figures 6, 7 and 8 and remove 3 single figures in total, we also revise the relevant text to comply with these new figures. In new Figures 6h, 7h and 8h, we show the annual zonal mean differences between normalized solar dimming and stratospheric aerosol geoengineering effects instead of the ratios between them. Most of the ratios showed in previous Figure 6h, 7h and 8h are close to value of one, but very large values occur when the denominators close to zero. With changing to show the differences between two normalized effects of geoengineering, we can avoid of this situation and better present the differences between solar dimming and stratospheric aerosol. Similar to new Figure 6h, 7h and 8h, we show the monthly climatological differences of normalized solar dimming effects and stratospheric aerosol effects in new Figure 6i, 7i and 8i. The previous Fig. 6j, 7j and 8j are removed in new figures as they deliver similar messages as Fig. 6i, 7i and 8i.

We define all normalization methods in Section 2: Data and methods, see the reply to another of the "general comment" below.

The following are new Figures 6, 7 and 8:

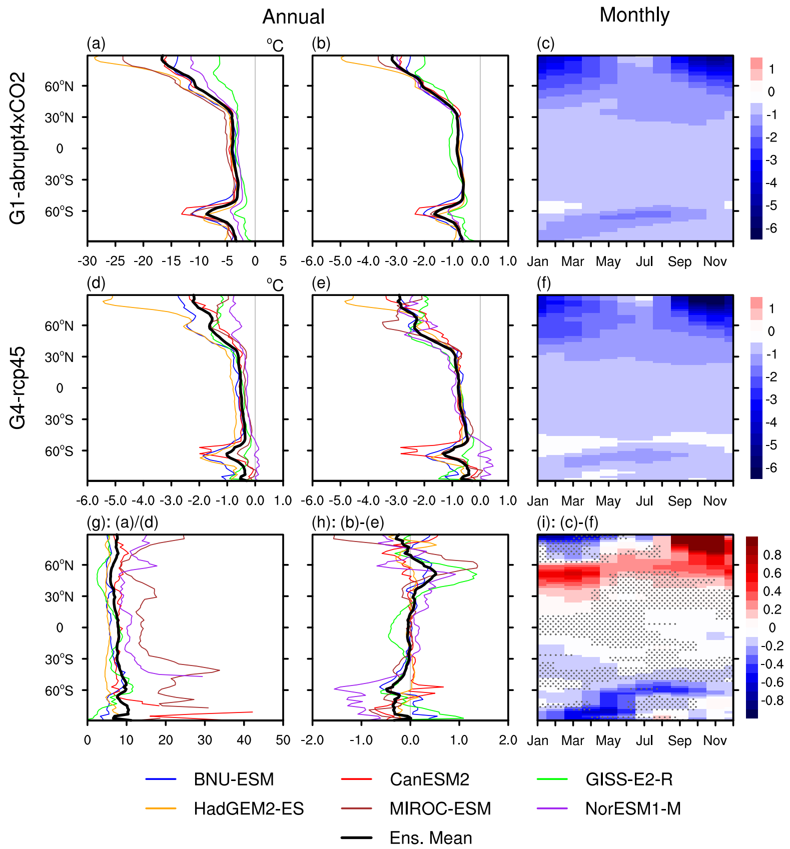

Figure 6: Absolute difference of annual zonal mean in the extreme low temperature TNn (left column), Normalized difference with respect to annual zonal mean (middle column) and monthly zonal mean (right column) in TNn: (a), (b), (c) G1 – abrupt4×CO2, (d), (e), (f) G4 – rcp45, (g) the ratio between absolute G1 – abrupt4×CO2 and G4 – rcp45, (h) the annual zonal mean difference between normalized G1 – abrupt4×CO2 and G4 – rcp45, (i) the monthly zonal mean difference between normalized G1 – abrupt4×CO2 and G4 – rcp45 taken over the 40-year analysis period. In panel (i) red colours indicate relatively greater changes with G4 and blue colours with G1, stippling indicates regions where fewer than 5 of 6 models agree on the sign of the model response. 3×3-point smoothing was applied to the seasonal-latitude change.

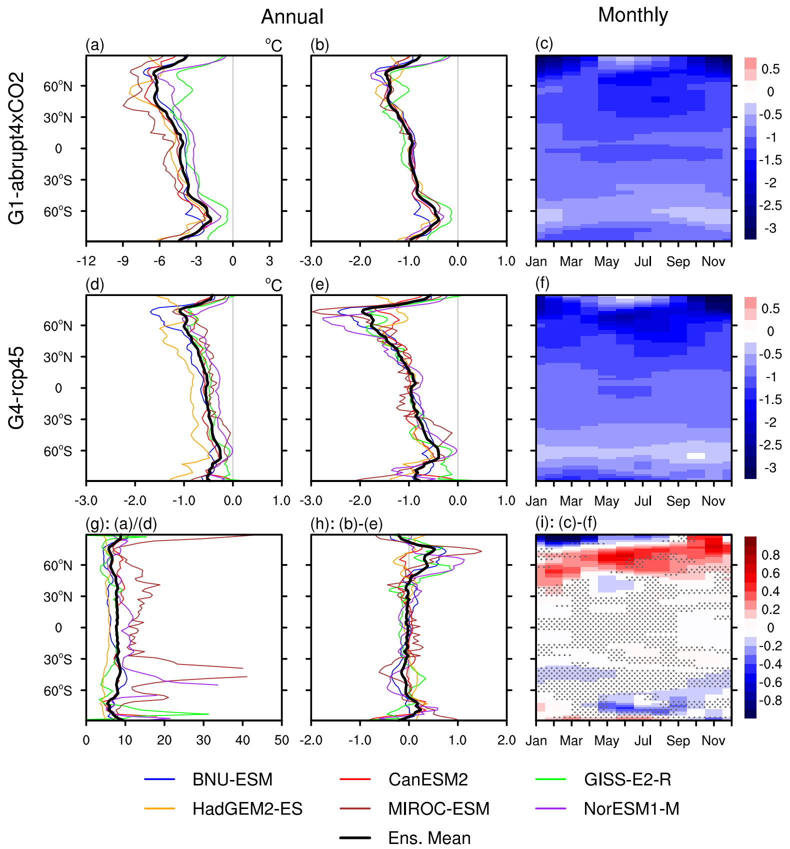

Figure 7: Absolute difference of annual zonal mean in the extreme high temperature TXx (left column), Normalized difference with respect to annual zonal mean (middle column) and monthly zonal mean (right column) in TXx: (a), (b), (c) G1 – abrupt4×CO2, (d), (e), (f) G4 – rcp45, (g) the ratio between absolute G1 – abrupt4×CO2 and G4 – rcp45, (h) the annual zonal mean difference between normalized G1 – abrupt4×CO2 and G4 – rcp45, (i) the monthly zonal mean difference between normalized G1 – abrupt4×CO2 and G4 – rcp45 taken over the 40-year analysis period. In panel (i) red colours indicate relatively greater changes with G4 and blue colours with G1, stippling indicates regions where fewer than 5 of 6 models agree on the sign of the model response. 3×3-point smoothing was applied to the seasonal-latitude change.

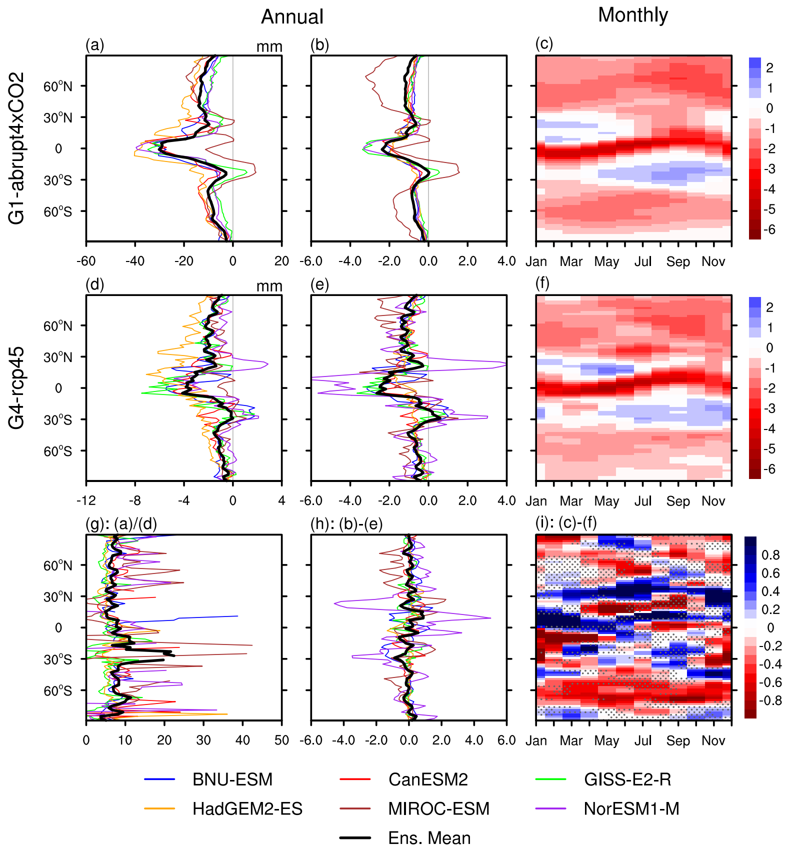

Figure 8: Absolute difference of annual zonal mean in the extreme precipitation Rx5day (left column), Normalized difference with respect to annual zonal mean (middle column) and monthly zonal mean (right column) in Rx5day: (a), (b), (c) G1 – abrupt4×CO2, (d), (e), (f) G4 – rcp45, (g) the ratio between absolute G1 – abrupt4×CO2 and G4 – rcp45, (h) the annual zonal mean difference between normalized G1 – abrupt4×CO2 and G4 – rcp45, (i) the monthly zonal mean difference between normalized G1 – abrupt4×CO2 and G4 – rcp45 taken over the 40-year analysis period. In panel (i) blue colours indicate relatively greater changes with G4 and red colours with G1, stippling indicates regions where fewer than 5 of 6 models agree on the sign of the model response. 3×3-point smoothing was applied to the seasonal-latitude change.

The paper will gain if the differences in the forcing of the two experiments are clearly stated in the beginning. Mean values of temperature and precipitation might also be helpful for the reader.

Reply: Thanks for this constructive suggestion. We reorder the results of "TOA net radiation flux" and "Probability distribution of monthly temperature and precipitation" with introducing the radiative forcing results firstly. For the differences in the forcing of the two experiments, we add the following part in the "Introduction":

Both methods would cool Earth's surface by reducing sunlight reaching the surface, either by aerosols reflecting sunlight or by artificially reducing the solar constant in climate models. The injected stratospheric aerosols under G4 not only scatter shortwave radiation, also absorb near infrared and longer wavelengths radiation (Lohmann and Feichter, 2005). The differences between stratospheric aerosol injection and solar dimming are influenced strongly by the absorption of longwave radiation by aerosols, this atmospheric heating imbalance could further stabilize the troposphere and lead to stronger precipitation reduction under stratospheric aerosol injection than under solar dimming (Niemeier et al., 2013).

Lohmann, U., and Feichter, J.: Global indirect aerosol effects: A review, Atmos. Chem. Phys., 5, 715–737, doi:10.5194/acp-5-715-2005, 2005.

Niemeier, U., Schmidt, H., Alterskjær, K., and Kristjánsson, J. E.: Solar irradiance reduction via climate engineering: Impact of different techniques on the energy balance and the hydrological cycle, J. Geophys. Res. Atmos., 118, 11905–11917, doi:10.1002/2013JD020445, 2013.

In the "TOA net radiation flux" part, we add:

The forcing of the G1 solar dimming and G4 stratospheric aerosol injection experiments are quite different, there can be a difference in the mean and extreme climate responses. The multi-model ensemble mean net radiation flux at top of atmosphere (TOA) is 2.76Wm^{-2} and 0.004 Wm^{-2} for the abrupt×4CO2 and G1 experiments, and 1.63 Wm^{-2} and 1.27 Wm^{-2} for the rcp45 and G4 experiments during their 40-year analysis period. Therefore, the G1 solar dimming and G4 stratospheric aerosol injection exert a reduction of 2.76 Wm^{-2} and 0.36 Wm^{-2} for net radiation fluxes at TOA respectively. The differences of mean net radiation flux at TOA over land and ocean between two geoengineering experiments and their reference experiments are show in Table 3.

We also revise Table 3 to present changes of net radiation flux at TOA instead of net shortwave radiation flux.

In the "Probability distribution of monthly temperature and precipitation" part we add:

The G1 solar dimming and G4 stratospheric aerosol injection geoengineering greatly affected the mean climate states. The annual mean surface air temperatures are 291.0 K and 286.7 K for abrupt4×CO2 and G1 experiments, 288.8 K and 288.3 K for rcp45 and G4 experiments respectively during their 40-year analysis period. The global hydrological strength is likewise reduced; the annual precipitation totals are 1125.8 mm and 1026.9 mm for abrupt4×CO2 and G1 experiments, 1098.4 mm and 1084.3 mm for rcp45 and G4 experiments (Table 3).

The hypothesis given in the abstract have to be better based on results and further explanations. You should avoid a propbably in the abstract. This is the place for new results. So yave should base the probably on results and you can give a clear answer. E.g. show that you see the claimed respose of the stratospheric dynamic in the results, like a change in the polar vortex.

Reply: Thanks for your constructive comment. We revise the abstract as the following:

We examine extreme temperature and precipitation under two potential geoengineering methods forming part of the Geoengineering Model Intercomparison Project (GeoMIP). The solar dimming experiment G1 is designed to completely offset the global mean radiative forcing due to a CO_2-quadrupling experiment (abrupt4×CO2), while in GeoMIP experiment G4, the radiative forcing due to the representative concentration pathway 4.5 (RCP4.5) scenario is partly offset by a simulated layer of aerosols in the stratosphere. Both G1 and G4 geoengineering simulations lead to lower minimum temperatures (TNn) at higher latitudes, and on land primarily through feedback effects involving high latitude processes such as snow cover, sea ice and soil moisture. There is larger cooling of TNn and maximum temperatures (TXx) over land compared with oceans, and the land-sea cooling contrast is larger for TXx than TNn. Maximum 5-day precipitation (Rx5day) increases over subtropical oceans, whereas warm spells decrease markedly in the tropics, and the number of consecutive dry days decreases in most deserts. The precipitation during the tropical cyclone (hurricane) seasons becomes less intense, whilst the remainder of the year becomes wetter. Stratospheric aerosol injection is more effective than solar dimming in moderating extreme precipitation (and flooding). Despite the magnitude of the radiative forcing applied in G1 being ~7.7 times larger than in G4, and differences in the aerosol chemistry and transport schemes amongst the models, the two types of geoengineering show similar spatial patterns in normalized differences of extreme temperatures changes. Large differences mainly occur at northern high latitudes, where stratospheric aerosol injection more effectively reduces TNn and TXx. While the pattern of normalized differences of extreme precipitation is more complex than that of extreme temperatures, generally stratospheric aerosol injection is more effective in reducing tropical Rx5day, while solar dimming is more effective over extra-tropical regions.

The forcings of the two experiment are very different. Therefore I recommend to normalize the results when possible add add this to the figures.

Reply: Thanks. In our new Figure 1 (we reorder some paragraph, previous Fig.2 is labelled as Fig. 1 now) and Figure 4, we show the normalized results. We normalize the values of each grid from the differences of G1-abrupt4xCO2 according to the global average of G1-abrupt4xCO2, same for G4-rcp45. With these normalized results, we present the difference between normalized G1-abrupt4xCO2 and G4-rcp45 instead of the ratio between non-normalized G1-abrupt4xCO2 and G4-rcp45 to avoid large unrealistic values. In Figure 6, 7 and 8, we also show the differences of zonally normalized results in several single figures instead of ratios between non-normalized fields. We define all normalization methods in Section 2: Data and methods as the following:

2.3 Normalization methods

There are large differences in forcing between the G1 solar dimming and G4 stratospheric aerosol injection geoengineering schemes. The mean and extreme climates under the two type geoengineering are quite different as will be shown below. To aid the comparisons, we adopt the following normalization methods to compare spatially relative effectivities between solar dimming and stratospheric aerosol injection.

The normalized global spatial effects of solar dimming or stratospheric aerosol injection are defined as the grid mean difference relative to the global mean difference:

$$< X^{geo} - X^{ref} >= \frac{\overline{X}^{geo}_{grid} - \overline{X}^{ref}_{grid}}{|\overline{X}^{geo}_{global} - \overline{X}^{ref}_{global}|}$$

where the operator <> denotes the normalized grid value, X is TXx, TNn, Rx5day or other climate field, an overbar denotes the average of each grid cell or the global average, the absolute operator || in the denominator of the right term preserves the sign of the geoengineering anomaly. The superscript "geo" represents geoengineering experiments of G1 solar dimming or G4 stratospheric aerosol injection, the superscript "ref" represents the reference experiments of abrupt4×CO_2 or rcp45.

To normalize zonal mean difference in the climate extreme indices relative to the global mean difference, we use a similar formula:

$$< X^{geo} - X^{ref} >= \frac{\overline{X}^{geo}_{zonal} - \overline{X}^{ref}_{zonal}}{|\overline{X}^{geo}_{global} - \overline{X}^{ref}_{global}|}$$

where the operator <> denotes the normalized zonal mean, an overbar denotes the zonal or global average, the absolute operator || in the denominator of the right term preserves the sign of the geoengineering anomaly.

The analyses in (Xia et al., 2017) and Niemeier et al (2013) on the differences of solar and aerosol forcing may provided som answers to these results, especially on the hyrological cycle.

Reply: Thanks for your constructive suggestions. We cite Niemeier et al. (2013) to explain the relatively stronger precipitation reduction under G4 stratospheric aerosol injection than that under G1 solar dimming.

The hydrological cycle strength weakens under both types geoengineering. In our analysis, the global mean precipitation decrease per Kelvin is stronger in response to G4 stratospheric aerosol than to G1 solar dimming. This is consistent with a previous study by Niemeier et al. (2013), in which impacts on energy balance and hydrological cycle by three different solar geoengineering schemes are examined. The differences between stratospheric aerosol injection and solar dimming are influenced strongly by the absorption of longwave radiation by aerosols, this atmospheric heating imbalance could further stabilize the troposphere and lead to stronger precipitation reduction under stratospheric aerosol injection than under solar dimming (Niemeier et al., 2013).

Based on the analysis on scaling of global mean precipitation reduction to mean temperature change (please check our reply to one of your “specific comments”), we add the following part in the "Discussion":

Recently Xia et al. (2018) found precipitation and evaporation changes are very similar under sulfate and solar dimming geoengineering schemes using the full tropospheric and stratospheric chemistry version of the Community Earth System Model (CESM). This is different from previous studies by Niemeier et al. (2013) and Ferraro et al. (2014), who found that the sulfate geoengineering has larger effect on the hydrological cycle. Xia et al. (2018) suggested that the column ozone change could possibly play an important role in a fully coupled atmosphere–chemistry model by changing radiative forcing and atmospheric lapse rate, while in Niemeier et al. (2013) and Ferraro et al. (2014) the same prescribed ozone was used in all scenarios. In our study, according to the scaling of global mean precipitation reduction to mean temperature change, all models show a relatively larger reduction of global mean precipitation per Kelvin under stratospheric aerosol injection than under solar dimming, which is consistent with Niemeier et al. (2013) and Ferraro et al. (2014). Among six GeoMIP models used here, only GISS-E2-R model calculates ozone for its G4 simulation, other models and experiments all use prescribed ozone. Therefore, we cannot diagnose ozone's roles as suggested by Xia et al. (2018).

Xia, L., Nowack, P. J., Tilmes, S., and Robock, A.: Impacts of stratospheric sulfate geoengineering on tropospheric ozone, Atmos. Chem. Phys., 17, 11913-11928, doi:10.5194/acp-17-11913-2017, 2017.

Specific comments

Page 2

Line 1: A hypothesis like this is not great in the abstract. You may better provide results.

Reply: Thanks. Done. Please refer to our previous reply to your general comment.

Line 7: Again, better avoid probably in the abstract. You can name the differences here in case they are significant.

Reply: Thanks. Done. Please refer to our previous reply to your general comment.

Line 24: In case you want to cite cloud brightening here, you should add Alterskjer et al (2013) with G5. But cloud brightning is not relevant for your topic.

Reply: Thanks. We rephrase this sentence to the following:
Kravitz et al. (2011, 2013c) defined a set of numerical SRM experiments under the Geoengineering Model Intercomparison Project (GeoMIP), comprising solar dimming experiments (G1 and G2), stratospheric aerosol injection simulations (G3 and G4) and marine cloud brightening experiments (G4cdnc, G4sea-salt).

Page 3
Line 5: Neither Geoengineering nor the future produce warming or cooling. Please rephrase.

Reply: We rephrase this sentence to the following:
Dagon and Schrag (2017) showed that solar geoengineering mitigates extreme heat events from greenhouse warming, though the regional response is variable in part due to varying soil moisture content: soils dry out over the course of the summer as daily maximum temperature increases, and this relationship is strengthened under solar geoengineering.

Page 4
Line 9: A number of the mean forcing would be good.

Reply: Thanks. We add the following sentence after Line 9:
The global temporally averaged forcing of the G1 solar dimming experiment ranges from -9.6 to -6.4 Wm^{-2}, and the G4 stratospheric aerosol experiment ranges from −3.6 to −1.6 Wm^{-2}, depending on the model (Schmidt et al., 2012; Kashimura et al., 2017).

Schmidt, H., Alterskjær, K., Bou Karam, D., Boucher, O., Jones, A., Kristjánsson, J. E., Niemeier, U., Schulz, M., Aaheim, A., Benduhn, F., Lawrence, M., and Timmreck, C.: Solar irradiance reduction to counteract radiative forcing from a quadrupling of CO2: climate responses simulated by four earth system models, Earth Syst. Dynam., 3, 63–78, doi:10.5194/esd-3-63-2012, 2012.
Kashimura, H., Abe, M., Watanabe, S., Sekiya, T., Ji, D., Moore, J. C., Cole, J. N. S., and Kravitz, B.: Shortwave radiative forcing, rapid adjustment, and feedback to the surface by sulfate geoengineering: analysis of the Geoengineering Model Intercomparison Project G4 scenario, Atmos. Chem. Phys., 17, 3339–3356, doi:10.5194/acp-17-3339-2017, 2017.

Page 5

Line 21: It is not clear to me if you calculate the PDF for the ensemble mean or for each model and average thereafter.

Reply: We calculate the PDF for each model and average thereafter. We rephrase the related sentence as the following to make it clear:

We computed the probability density functions (PDFs) of temperature and precipitation for each model and average all models thereafter to get a general idea of the changes in the two geoengineering experiments (G1 and G4) compared to their baseline experiments (abrupt4×CO2 and rcp45).

Line 24/25: Reformulate to include both experiments.

Reply: Done.

Page 8
1st paragraph: Forcing differences to the control run are much stronger in G1 than in G4. Readers not familiar with this experiments may not realize this right away. You may add a figure to highlight this differences, e.g. time series or give a number of the forcings earlier in the text. OK, you do later. Maybe you reorder your paragraphs.
How different are the PDF results to Curry et al?

Reply: Thanks for your constructive suggestion. We reorder the results of 3.1 ("Probability distribution of monthly temperature and precipitation") and 3.2 ("TOA net radiation flux") to present the radiative forcing results firstly. In section 2 ("Data and Methods") we refer to Schmidt et al. (2012) and Kashimura et al. (2017) to show the large differences in forcing exerted by G1 solar dimming and G4 stratospheric aerosol geoengineering. In this paragraph we give the numbers of net radiative flux reduction due to G1 solar dimming and G4 stratospheric aerosol geoengineering methods. Please refer to our previous replies to your general comments.

The PDFs results in our study are different to Curry et al. (2014). Curry et al. (2014) use the piControl as the reference experiment and compare the PDFs of G1 with piControl, which suggests temperature and precipitation perturbations that occur under abrupt4 × CO2 are all reduced to near-piControl values by G1-type geoengineering. In our study, we choose abrupt4×CO2 as the reference for G1 and rcp45 as the reference for G4. We try to show how the global mean and extreme temperature and precipitation can be ameliorated by G1 solar dimming and G4 stratospheric aerosol injection. We add the following to clarify:

The PDFs for G1 and abrupt4×CO2 differ from those presented by Curry et al. (2014) as expected, due to the different choice of reference simulation. Curry et al. (2014) use the piControl as the reference experiment and compare the PDFs of G1 with piControl, which suggests temperature and precipitation perturbations that occur under abrupt4×CO2 are all reduced to near-piControl values by G1 solar dimming geoengineering. In our study, we choose abrupt4×CO2 as the reference for G1, and rcp45 as the reference for G4, as we aim to investigate how the global mean and extreme temperatures and precipitation events may be ameliorated by G1 solar dimming and G4 stratospheric aerosol injection geoengineering compared to global warming.

Line 14: TOA forcing (SW +LW) is more general than SW at the surface. For sulfate CE the LW part is important. In case TOA forcing adds some information, you may add this to Figure 2.

Reply: Thanks. We revise the Figure 2 to show the differences of TOA SW+LW forcing. At the same time, the panel (c) shows the difference between normalized TOA net radiation fluxes of G1-abrupt4xCO2 and G4-rcp45, instead of non-normalized ratios between G1-abrupt4xCO2 and G4-rcp45. As we reorder the sections 3.1 and 3.2, this new figure is labeled as Figure 1. We define the normalization methods in Section 2: Data and methods. Please refer to our previous replies on normalization methods.

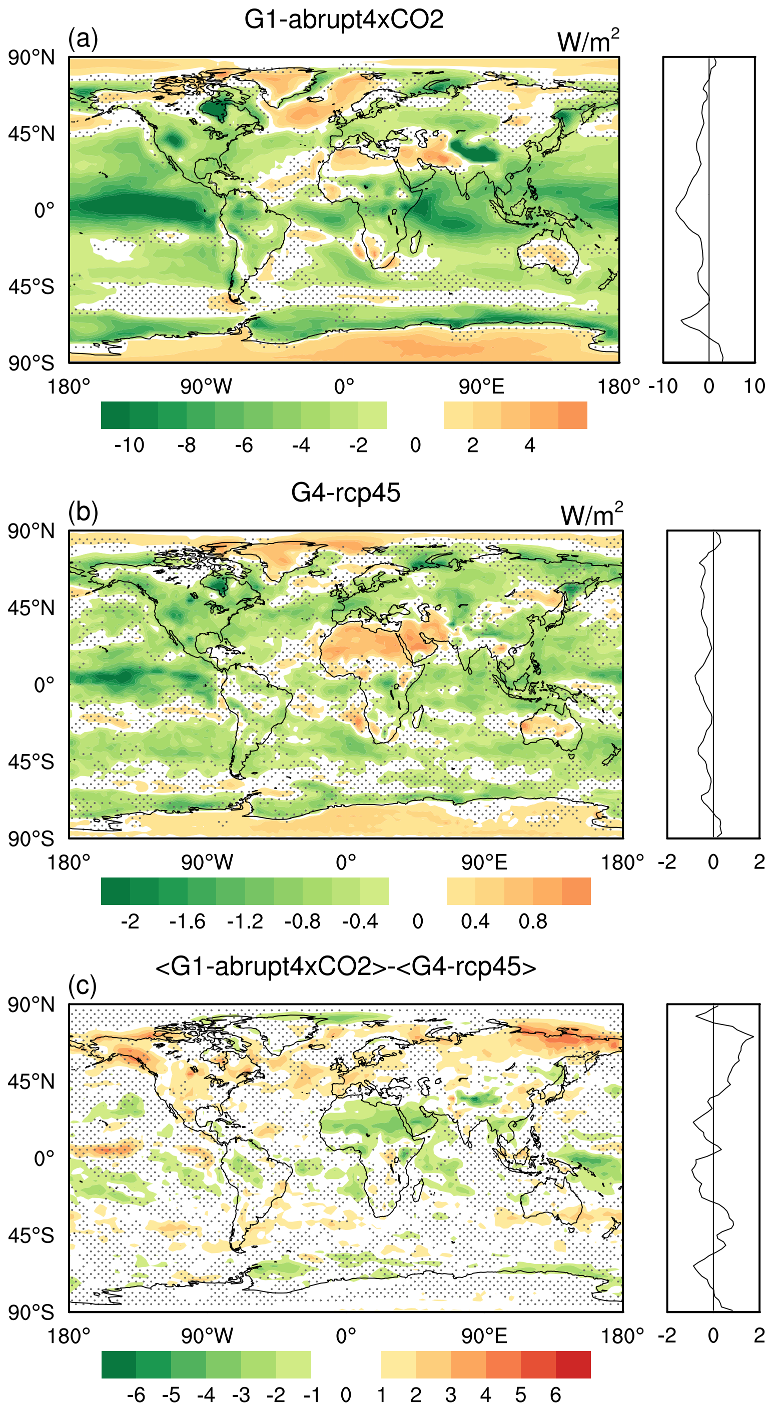

Figure 1: Geographical distributions over the 40-year analysis periods of differences in net radiation flux at TOA between G1-abrupt4×CO2 (top), G4-rcp45 (middle). The bottom panel shows the differences in net radiation flux at TOA between normalized G1-abrupt4×CO2 and G4-rcp45 Stippling indicates regions where fewer than 5 of 6 models agree on the sign of the model response. The right sub-panels show the zonal average of the left sub-panels. Note that all three panels have different scales.

We also revise the relevant section (3.1 TOA net radiation) as the following:

The multi-model ensemble mean net radiation flux at the top of atmosphere (TOA) is 2.76Wm^{-2} and 0.004 Wm^{-2} for abrupt×4CO2 and G1 experiments, and 1.63 Wm^{-2} and 1.27 Wm^{-2} for rcp45 and G4 experiments during their 40-year analysis periods. Therefore, the G1 solar dimming and G4 stratospheric aerosol injection exert a reduction of 2.76 Wm^{-2} and 0.36 Wm^{-2} for net radiation fluxes at TOA respectively. The differences of mean net radiation flux at TOA over land and ocean between two geoengineering experiments and their reference experiments are show in Table 3. Although the ratio between the global temporally averaged net radiation flux reductions at TOA is a factor of ~7.7, the spatial distribution of net radiation flux changes for the G1 and G4 ensemble means are quite similar, especially the positive TOA net radiation over Greenland, Antarctica, North Africa and West Asia, and the negative TOA net radiation over North America, Central Europe and tropical ocean basins (Figure 1). The entire ensemble shows a large and consistent positive TOA net radiation east of Greenland in the North Atlantic under G1 solar dimming (Figure 1a), the region associated with the overturning part of the Atlantic meridional circulation (AMOC), and which under the G1 forcing was shown to be strongly affected by changes in radiative forcing and air/ocean heat exchange (Hong et al., 2017). However, differences are clearer when we investigate the spatial pattern of normalized effects exerted by the two SRM experiments, although most regions have differences close to zero for normalized solar dimming and stratospheric aerosol geoengineering effects on TOA net radiation (Figure 1c). The G4 stratospheric aerosol injection geoengineering introduces a more effective reduction in TOA net radiation over the Northern Hemisphere, especially over the high-latitude continents, such as northern North America, Siberia and some regions of western Europe. The G1 solar dimming geoengineering introduces a more effective reduction in TOA net radiation over North Africa, northern South America, the Indian Ocean and tropical Western Pacific. In contrast, many other equatorial regions, the Southern Ocean and the Intertropical and South Pacific Convergence Zones display small differences between normalized solar dimming and stratospheric aerosol injection effects.

The models show more consistent responses under G1 solar dimming then under G4 stratospheric aerosol injection, which is probably due to smaller signal-to-noise ratios under G4. The models are inconsistent under both G1 and G4 over the Southern Ocean around Antarctica, where CMIP5 models also show large uncertainties in cloud radiative effects (Stocker et al. 2013). These results suggest that solar dimming and stratospheric aerosol injection geoengineering forcing may affect clouds differently in some models: low level clouds are important for radiative surface fluxes in the North Atlantic where differences between G1 and G4 are positive, while higher clouds are more important in the deep tropical convection regions where differences are weakly negative. It is also possible that the different mean climate states between G1 and G4, and surface albedo changes due to sea ice and snow cover are responsible for the large differences in net radiation flux in the coastal Antarctic seas, and the more modest differences seen in the North Atlantic and Barents Sea along with Alaska and eastern Siberia.

In addition to different mean climate states and cloud responses, there are numerous sources of inter-model differences in response to solar dimming and stratospheric aerosol geoengineering. The G1 solar dimming assumes global uniform solar reduction, while under G4 sulphate aerosols are handled differently among the participating models. GISS-E2-R and HadGEM2-ES adopt stratospheric aerosol schemes to simulate the sulfate aerosol optical depth (AOD), BNU-ESM and MIROC-ESM use the prescribed meridional distribution of AOD recommended by the GeoMIP protocol, CanESM2 specifies the uniform sulfate AOD (Kashimura et al., 2017).

NorESM1-M specifies the AOD and effective radius which were calculated in previous simulations with the aerosol microphysical model ECHAM5-HAM (Niemeier et al., 2011, Niemeier and Timmreck, 2015). Although a prescribed AOD can be set, difference in assumed particle size for the stratospheric sulfate aerosols (Pierce et al., 2010) and the warming effects of stratospheric aerosol (Pitari et al., 2014) cause difference in the SRM forcing.

Niemeier, U. and Timmreck, C.: What is the limit of climate engineering by stratospheric injection of SO2? Atmos. Chem. Phys., 15, 9129 – 9141 doi:10.5194/acp-15-9129-2015, 2015.

Pierce, J. R., Weisenstein, D. K., Heckendorn, P., Peter, T., and Keith, D. W.: Efficient formation of stratospheric aerosol for climate engineering by emission of condensible vapor from aircraft, Geophys. Res. Lett., 37, L18805, doi:10.1029/2010GL043975, 2010.

Pitari, G., Aquila, V., Kravitz, B., Robock, A., Watanabe, S., Cionni, I., Luca, N. D., Genova, G. D., Mancini, E., and Tilmes, S.: Stratospheric ozone response to sulfate geoengineering: Results from the Geoengineering Model Intercomparison Project (GeoMIP), J. Geophys. Res.-Atmos., 119, 2629–2653, 2014.

Line 25: In case you talk about single models you may take into account that the forcing from the sulfate layer may be very different between the models (see (Pitari et al., 2013))

Reply: Thanks. We add the following sentences in the revised section 3.1 on TOA net radiation:
The G1 solar dimming assumes global uniform solar reduction, while under G4 sulphate aerosols are handled differently among the participating models. GISS-E2-R and HadGEM2-ES adopt stratospheric aerosol schemes to simulate the sulfate aerosol optical depth (AOD), BNU-ESM and MIROC-ESM use the prescribed meridional distribution of AOD recommended by the GeoMIP protocol, CanESM2 specifies the uniform sulfate AOD (Kashimura et al., 2017). NorESM1-M specifies the AOD and effective radius which were calculated in previous simulations with the aerosol microphysical model ECHAM5-HAM (Niemeier et al., 2011). Although a prescribed AOD can be set, difference in assumed particle size for the stratospheric sulfate aerosols (Pierce et al., 2010) and the warming effects of stratospheric aerosol (Pitari et al., 2014) cause difference in the SRM forcing.

Page 9
Line 2/3: Climate under G1 is pre-industrial while G4 is 2020. This can play a role here.

Reply: Yes, we revise this sentence as following:
It is also possible that the different mean climate states between G1 and G4, and surface albedo changes due to sea ice and snow cover are responsible for the large differences in net radiation flux in the coastal Antarctic seas, and the more modest differences seen in the North Atlantic and Barents Sea along with Alaska and eastern Siberia.

Figure 2: I wonder about the hatching in c). Only small areas with values close to one are significant. Is this correct and do you have an explanation?

Reply: In the previous Figure 2c, we defined the significant change as larger than the 95th or smaller than the 5th percentile threshold value of the ratios between non-normalized G1-abrupt4xCO2 and G4-rcp45 for TOA net shortwave radiation fluxes from all model grids. In the new revised figure (Figure 1 in the revised manuscript), we show the TOA SW+LW forcing of G1-abrupt4xCO2 and G4-rcp45 in Figure 1a and 1b, and the differences between normalized G1-abrupt4xCO2 and G4-rcp45 in Figure 1c. Now the stippling indicates regions where fewer than 5 of 6 models agree on the sign of the model response. By showing the differences between normalized G1-abrupt4xCO2 and G4-rcp45, we can better present the non-uniform regional responses between G1 solar dimming and G4 stratospheric aerosol geoengineering methods.

In the new Figure 1c, we find G4 stratospheric aerosol geoengineering introduces a more effective reduction in TOA net radiation over northern hemisphere, especially over the high-latitude continents, such as north of Northern America, Siberia and some regions of western Europe. This pattern of consistent responses in new Figure 1c is similar to hatching areas where the ratios are significantly small (therefore large reduction in net radiation in G4) in the previous Figure 2c.

Page 11

Figure 3: You may add some words that Rx5days and G4 is partly positive, increase in precipitation, which indicates nicely the climate variability.

Reply: Thanks. We add a sentence to clarify it:

In contrast, the index for G4-rcp45 (Fig.3f) is near-zero, though slightly negative on the whole, with the multi-model mean value of -1.8±0.9 mm. The partly positive Rx5day for G4-rcp45 reflects the climate variability simulated by models and lower signal-to-noise ratio.

Page 12

Line 2: Do mean values of p and t scale the same in G1 and G4?

Reply: The scaling of mean precipitation and mean temperature is not same in G1 and G4. But the scaling of extreme precipitation represented by Rx5Dday and mean temperature is almost same if one model is excluded. We elaborate these in the main text as following:

If relative humidity and atmospheric circulation remain relatively unchanged, then intense precipitation amount is governed by total precipitable water in the atmosphere, which the Clausius–Clapeyron relation says scales with mean temperatures (Allen and Ingram, 2002). The global mean precipitation decreases 2.1±0.4% per Kelvin in response to G1 solar dimming, and 2.7±1.0% per Kelvin in response to G4 stratospheric aerosol injection. The GISS-E2-R model contributes a relatively large portion to the spread of scaling between mean precipitation and temperature with a value of 4.5% per Kelvin for G4. If excluding the GISS-E2-R model, the global mean precipitation decreases 2.0±0.4% per Kelvin in response to G1 solar dimming, and 2.3±0.5% per Kelvin in response to G4 stratospheric aerosol injection. The scaling between mean precipitation and mean temperature under G1 and G4 is smaller than 3.4% precipitation change per Kelvin estimated from other coupled models under long-term equilibrium climate in response to doubling CO_2 (Allen and Ingram, 2002). The global mean Rx5day decreases 3.4±1.0% per Kelvin in response to G1 solar dimming, and 4.3±2.6% per Kelvin in response to G4 stratospheric aerosol injection. GISS-E2-R gives global mean Rx5day decreases 9.5% per Kelvin for G4. If excluding GISS-E2-R model, the global mean Rx5day decreases 3.4±1.1% per Kelvin in response to G1 solar dimming, and 3.3±0.6% per Kelvin in response to G4 stratospheric aerosol injection. The scaling of mean precipitation and mean temperature is expected to be much less than the 6.5% per Kelvin implied by the Clausius–Clapeyron relation, as the global-mean precipitation is primarily constrained by the availability of energy not moisture (Pall et al., 2007). The scaling of Rx5day and mean temperature under G1 and G4 is close to, but still weaker than the Clausius–Clapeyron relation, probably because Rx5day is not really an index of the heaviest rainfall events that are expected to be constrained by the Clausius–Clapeyron relation. The Clausius–Clapeyron relation implies the same scaling of extreme precipitation and mean temperatures under both G1 and G4 experiments, which is the case here for five of six models, but not the GISS-E2-R model.

Allen, M. and Ingram, W.: Constraints on future changes in climate and the hydrologic cycle, Nature, 419, 224–232, 2002.
Pall, P., Allen, M. R., and Stone, D. A.: Testing the Clausius–Clapeyron constraint on changes in extreme precipitation under CO2 warming, Climate Dyn., 28, 351–363, doi:10.1007/ s00382-006-0180-2, 2007.

Fig 4: Please add normalized values here. You may normalize with mean T and P or with the TOA forcing difference G1-4xCO2 and G4-RCP45.
I am not sure I understand what you did in Fig 4i) You may add an equation. Again, hatching and significance seem not to fit. Are this area not significant? Otherwise your area with significant results is very small and you should discuss the relevance of your results in this case.

Reply: Thanks. Now we show normalized differences between G1-abrupt4xCO2 and G4-rcp45 in Figure 4c, 4f and 4i instead of ratios of non-normalized G1-abrupt4xCO2 and G4-rcp45. Stippling in all single figures indicate regions where fewer than 5 of 6 models agree on the sign of the model response. Although the old Figure 4c, 4f and 4i use the hatching indicates significant change (larger than the 95th or smaller than the 5th percentile threshold value), the regions of significant change are similar to the new Figure 4c, 4f and 4i where models show consistent responses. For example, Northern North America, Western Europe in Figure 4c, Central Europe and Siberia in Figure 4f.

In the main text, we add the following sentences to clarify:
The stratospheric aerosol injection more effectively reduces the TNn in northern North America and western Europe compared with solar dimming, while the solar dimming more effectively reduces TNn in the Siberian coastal region, Eastern Antarctica and the adjacent ocean regions. The stratospheric aerosol also effectively reduces the TXx in northern North America and central Europe compared with solar dimming, but with a smaller spatial extent and magnitude compared with TNn. Stratospheric aerosol is more effective at reducing TXx in the Siberian coastal region, while the solar dimming seems more effective on reducing TNn there. ……
The difference between normalized change of G1-abrupt4×CO2 and G4-rcp45 is noisy and without coherent patterns (Fig. 4i).

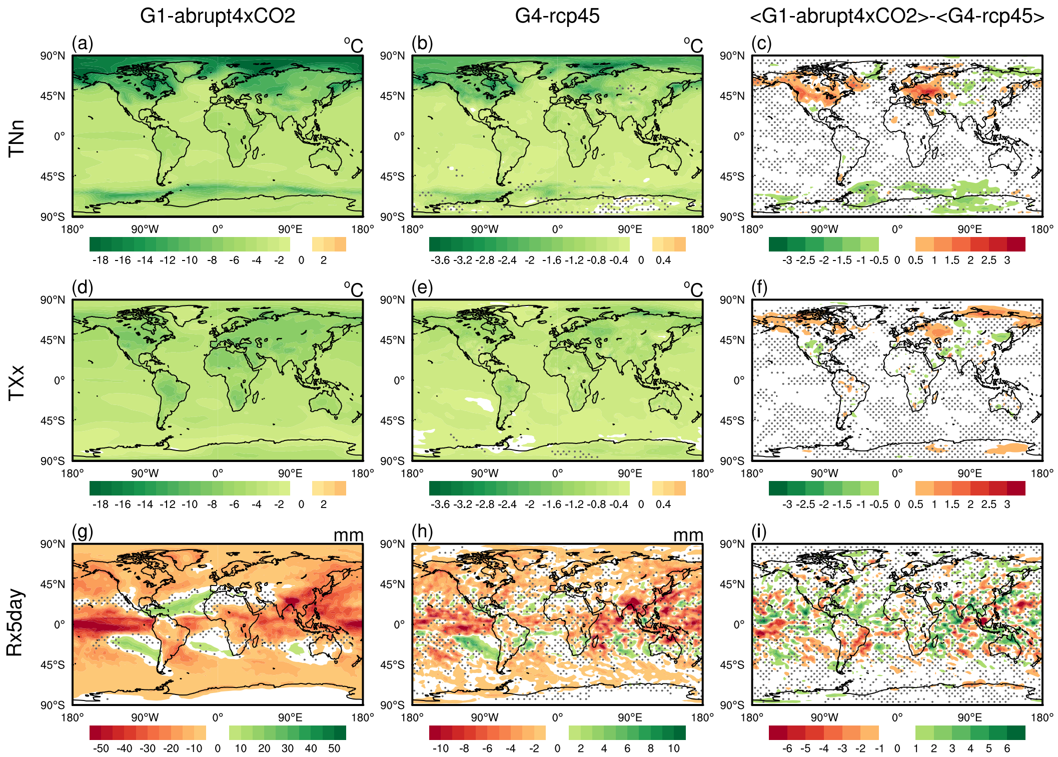

Figure 4: Geographical distributions over the 40-year analysis periods of the differences G1 - abrupt4×CO2 (left column), G4 - rcp45 (middle column), and differences between normalized G1 - abrupt4×CO2 and G4 - rcp45 (right column) for the extreme indices TNn (top row), TXx (middle row), and Rx5day (bottom row). Stippling indicates regions where fewer than 5 of 6 models agree on the sign of the model response. Note that panels have different colour scales.

Page 13

Line 6 to 16: You give a list of related topics here but I miss the clear relation to your results.

Reply: The discussion in this section refers to reasons why we see "the signature of polar amplification evident in both hemispheres but primarily in the Arctic" (lines 4-5 on page 13). We try to resolve this by modifying the text to:

The cooling patterns seen for TNn (Fig. 4a,b) are similar but with a larger signal for G1-abrupt4×CO2 than G4-rcp45, with the signature of polar amplification evident in both hemispheres but primarily in the Arctic. Several studies have considered the reasons behind this effect.

Line 17 to 24: The paper would gain of you can explain this feature better

Reply: Thanks. We revise this paragraph to the following to better explain the land-sea contrast differences between TXx and TNn:

A notable feature in Fig. 4a, 4b, 4d and 4e is the larger cooling of TNn and TXx over land compared with oceans, also expressed in Table 3. The land-sea cooling contrast is larger for TXx than TNn (Fig 4d, e; Table 3), and TXx shows more uniform cooling than TNn across all latitudes. This feature is consistent with the stronger relationship of shortwave forcing to TXx. Under GHG warming scenarios, heat capacity differences, contrasts in surface sensible and latent fluxes, and boundary layer differences lead to contrasts opposite to those under G1 and G4

(Sutton et al., 2007; Joshi et al., 2008). Under G1 and G4, GHG warming occurs 24 hours a day, while reduced solar radiation is more effective in reducing day-time temperatures (TXx), with the land-sea heat capacity differences further enhancing TXx over TNx. The land–sea cooling effects under G4-rcp45 (Fig 4b,4e) are consistent with Volodin et al. (2011) who found increased land–sea cooling contrast in annual mean temperature using the INMCM model forced with 4 Mt S/year equatorial stratospheric aerosol injection.

Line 28: 'Except Eastern China' this is a very small area. I guess this is a regional feature which is usually not very well represented in the models. Otherwise an explanation would be great.

Reply: Agreed. We delete this part and revise the sentence to:
The pattern is similar in G4-rcp45 but with a smaller magnitude.

Line 29: Better use solar dimming and stratospheric aerosol here also, so decide for one naming and stick to it.

Reply: Agreed. We also change other places to make it consistent.

Page 14
Line 11 to 13: I got lost. Can I see this in any figure?

Reply: We revise this sentence to the following:
The ensemble means show that Rx5day is strongly reduced over equatorial regions, especially in the equatorial Pacific and southern flank of the Tibetan Plateau (Fig. 4g,h).

Line 17/18: As you mention them, you may summarize the more complex interactions.

Reply: Thanks. We revise the part as the following:
This has been attributed to a weaker Hadley cell due to weaker radiative forcing (Tilmes et al., 2009), but more recent analysis of the tropical circulation suggests more complex interactions between radiative forcing and Hadley cell extent and intensity. Under GeoMIP G1 experiment, the Hadley cell edges remain at their preindustrial width latitudinally, despite the residual stratospheric cooling associated with elevated carbon dioxide levels (Davis et al., 2016; Guo et al., 2018). The damping of the seasonal migration of the Intertropical Convergence Zone (ITCZ) within the Hadley cell under G1 is associated with preferential cooling of the summer hemisphere (Smyth et al., 2017).

Line 28: Can you show this in a figure, link to existing figure or literature. In general, the small signal to noise ration is important for G4.

Reply: Thanks. We elaborate this line and its context as the following:
Furthermore, monsoonal regions including East Asia and India exhibit a reduction in Rx5day under G1-abrupt4×CO_2, which may be attributed to a weakened monsoon. Tilmes et al. (2013) observed, using a larger ensemble of models, that G1-abrupt4×CO_2 results in a robust decrease in monsoonal precipitation, while it increases under abrupt4×CO_2. Reduced Rx5day over monsoon regions is an indicator of weakened monsoon (Fig. 4g), because although the extreme precipitation index is calculated on an annual basis, it is dominated by wet

season precipitation, particularly in monsoon areas (Klein Tank et al., 2006). However, the change under G4-rcp45 is not as robust (Fig. 4h), due at least partially to lower mean temperature changes and land-sea thermal contrast, and therefore smaller signal-to-noise ratios compared with G1-abrupt4×CO2.

Klein Tank, A. M. G., Peterson, T. C., Quadir, D. A., Dorji, S., Zou, X., Tang, H., Santhosh, K., Joshi, U. R., Jaswal, A. K., Kolli, R. K., Sikder, A. B., Deshpande, N. R., Revadekar, J. V., Yeleuova, K., Vandasheva, S., Faleyeva, M., Gomboluudev, P., Budhathoki, K. P., Hussain, A., Afzaal, M., Chandrapala, L., Anvar, H., Amanmurad, D., Asanova, V. S., Jones, P. D., New, M. G., and Spektorman, T.: Changes in daily temperature and precipitation extremes in central and south Asia, J. Geophys. Res., 111, D16105, doi:10.1029/2005JD006316, 2006.

Page 17
Line 1 to 5: The forcing varies stronger in G4 between the models than in G1. In case a model simulates of provides most sulfate in the tropics cooling at the poles would be relatively low. You may show TOA of the single models in an appendix.

Reply: Yes. We show the TOA net radiation flux differences of G1-abrupt4×CO2 and G4-rcp45 for each model as Figure S1 and S2. We also add the following sentences to further clarity this point:

The spatial pattern of the TOA net radiation flux varies relatively more in G4-rcp45, ranging from -0.22 to -0.56 Wm^{-2}, while comparatively ranging from -2.29 to -3.40 Wm^{-2} in G1-abrupt4×CO2 (Figure S1, S2). As simulation of sulphate aerosols differs among the participating G4 models, the spatially varying forcing results in very different cooling patterns particularly at high latitudes.

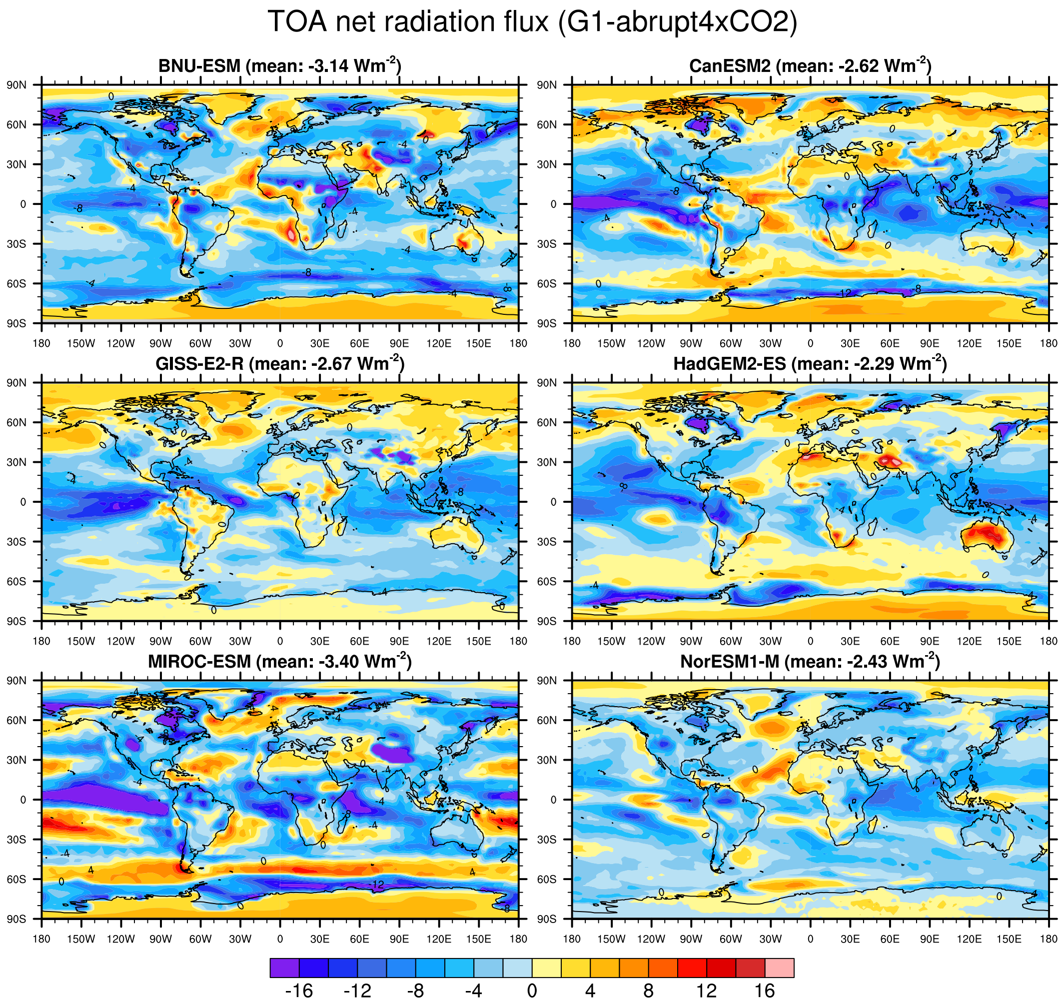

Figure S1: Geographical distributions over the 40-year analysis periods of the differences G1 - abrupt4×CO2 for TOA net radiation flux for BNU-ESM, CanESM2, GISS-E2-R, HadGEM2-ES, MIROC-ESM and NorESM1-M.

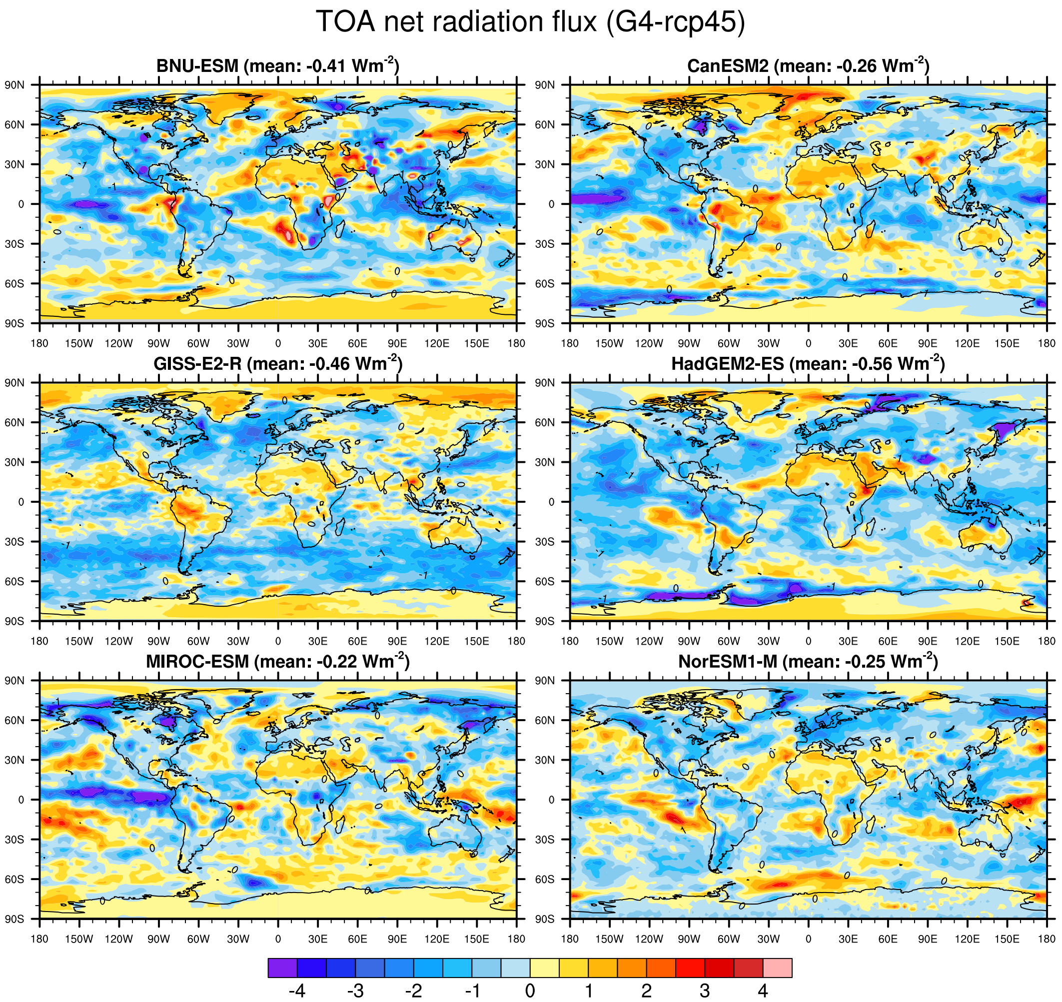

Figure S2: Geographical distributions over the 40-year analysis periods of the differences G4 – rcp45 for TOA net radiation flux for BNU-ESM, CanESM2, GISS-E2-R, HadGEM2-ES, MIROC-ESM and NorESM1-M.

Line 9: Better cite Schmidt et al, 2012 or Kravitz et al, 2013 here. They have shown the shift of the ITCZ.

Reply: Actually Kravitz et al. (2013) does not mention the effect, and Schmidt et al. (2012) notes that "While in HadGEM2-ES the zonally averaged position of the main branch of the ITCZ remains almost unchanged, it shifts slightly equatorward in the other three models" and "except for a small band slightly north of the equator over the Pacific which indicates an equatorward shift of the ITCZ in three of four models as mentioned above". They do not look at seasonality which is what we specifically talk about in this section, we change the text as:

This may be related to the reduced latitudinal extent of seasonal movement of the ITCZ under G1 as noted in previous studies (Schmidt et al., 2012; Smyth et al., 2017).

Line 15: Any explanation for the different results over central Asia. This results is also different to Aswathy et al (2015).

Reply: Aswathy et al. (2015) compared the sea-salt seeding experiments, sulfate injection experiments and RCP4.5 experiments during 2040-2069 to the RCP4.5 experiments during 2006-2035 control period, this is different from our comparison in this study, we compared the same period of 2030-2069 for G4 and RCP4.5. Aswathy et al. (2015) prescribe the radiative forcing to remain at the 2020 levels implied by the anthropogenic climate change under the RCP4.5. While in our study, we used the GeoMIP G4 simulation results, in which a constant 5Tg per year of SO_2 is introduced into the lower tropical stratosphere of climate models during the period of 2020-2069, while greenhouse gas forcing is defined by the RCP4.5 scenario.
In the previous version of this manuscript, we made a mistake in visually interpreting part of the results based on Figure 5e and 5f with Figure 4g and 4h. Now we reverse the colorbar of Figure 4g and 4h to make it clearer for comparing, and revise this paragraph as following:
The equatorial Pacific in the vicinity of the ITCZ displays increases in CDD under G1-abrupt4×CO2 at the same locations (Fig. 5e) as Rx5day decreases (Fig. 4g). This may be related to the reduced latitudinal extent of seasonal movement of the ITCZ under G1 as noted in previous studies (Schmidt et al., 2012; Smyth et al., 2017). Anti-correlation between CDD and Rx5day can also be seen for decreases in CDD and increases in Rx5day in the tropical Atlantic, South Atlantic and the southeast Pacific dry zone. Both northern and southern high latitudes, and large parts of Eurasia display increases in CDD and decreases in Rx5day (Fig. 5e, 4g). CDD decreases in the desert regions of northern Africa, southwestern Africa, Australia and southwestern North America, which are strongly influenced by the descending branch of the tropical Hadley cell. This implies most places have fewer droughts under the geoengineering simulation than without it. Fig. 5f shows that the pattern in G4-rcp45 is similar to G1-abrupt4×CO2 but noisier.

Page 18
Fig 6: I am not sure I understood how you normalize the right column. I understood (i) as b/e and (j) as c-f. But than the pattern should be similar.
Increase the contrast of Fig (c) and (f), thus darker blue.
Can you add significance to (i) and (j)? Values around 1 and 0 should be white (also in Fig 7 and 8)

Reply: Thanks. These suggestions largely improved our figures on showing monthly zonal differences between solar dimming and stratospheric aerosol geoengineering. Please check the new Figure 6, 7 and 8 in our replies to your general comments.
We remove the previous Fig (j) and plot the new Fig (i) as the difference between Fig (c) and Fig (f), Fig (c) and Fig (f) represent normalized response of solar dimming geoengineering relative to abrupt4xCO2 and stratospheric aerosol injection geoengineering relative to rcp45, so that (c) and (f) can be compared directly. We use darker blue or red for the right column sub-figures for Figure 6, 7 and 8. We also use white color to represent values around zero as you suggested.

Page 19
Line 8: Which figure? Cannot see this in 6c) or 6f).

Reply: We expand this sentence more clearly as the following:
The annual zonal mean pattern of G4-rcp45 (Fig. 6d) is comparable to G1-abrupt4×CO2 (Fig. 6a), but weaker by a factor of 7 to 9 in terms of their absolute magnitudes (Fig. 6g).

Line 18: 'affected more by solar dimming....' Where? It is largely blue. I may not get all positive and negative changes right. You may explain this a bit more.

Reply: In the newly revised Figure 6i, the differences in normalized G1-abrupt4×CO2 and G4-rcp45 (i.e. Fig. 6i) shows the difference between Fig. 6c and Fig. 6f. The negative values (blue colors) indicate relatively greater changes with G1, the positive values (red colors) indicate relatively greater changes with G4. Therefore, this sentence holds for the new Fig. 6i as well, and we further expand it to include spring season.
Fig. 6i shows that TNn in the northern high latitude springs and summers is affected much more by solar dimming than by stratospheric aerosol injection.

Line 19: Quit dark red around 60S

Reply: Thanks for pointing this out. We increase the contrast of Fig. 6i. In the new Fig. 6i, darker red represents relatively large change of G4 and darker blue represents large change of G1. Therefore, the blue occurring in the wintertime and springtime Southern Ocean around 60S suggests the TNn affected more by solar dimming than by aerosol injection, and it's similar to the springtime and summertime of northern high latitudes. We revise it as follows:
Fig. 6i shows that TNn in the northern high latitude springs and summers is affected much more by solar dimming than by stratospheric aerosol injection. A similar response is also present in the wintertime and springtime Southern Ocean. The only regions where stratospheric aerosol injection induces a significantly larger response than solar dimming is in the high Arctic in winter and latitudes between 40^{o}-60^{o}N in spring and winter, suggestive of a longwave radiative effect of the aerosols.

Page 21

Line 9 to 15: You are on quite weak ground here. The polar stratospheric vortex may weaken due to less sea ice and more wave propagation, sulfate warming the stratosphere may strengthen the vortex (Ferraro et al, 2014) etc.

Reply: Yes. We revise this part as the following:
Fig. 7i suggests that the relative effectiveness of stratospheric aerosols and solar dimming is similar, except for the Arctic, and perhaps Antarctica, where aerosols appear more effective than dimming in winter. Since the lack of shortwave radiative forcing during winter would not lead to differences in solar dimming or aerosol response, atmospheric circulation changes are implicated. The tropical lower stratospheric radiative heating due to stratospheric aerosol would drive a thermal wind response, which would intensify the stratospheric polar vortices. In contrast, solar dimming does not produce this effect, and so there is little intensification of the polar vortex in G1. Therefore, the response of the northern hemisphere polar vortex to solar dimming geoengineering is much weaker than under stratospheric aerosol injection (Ferraro et al. 2015). A strengthening of the wintertime stratospheric polar vortices occurs under G4, tending to cool polar surface temperatures, which is consistent with wintertime northern hemisphere TNn and TXx patterns shown in Fig. 6i and 7i.

Ferraro, A. J., Charlton-Perez, A. J. and Highwood, E. J.: Stratospheric dynamics and midlatitude jets under geoengineering with space mirrors and sulfate and titania aerosols, J. Geophys. Res. Atmos., 120, 414–429, doi:10.1002/2014JD022734, 2015.

Page 23

Line 16: Yes, but this depends also on the meridional distribution of the aerosols which is not given in the paper and may be different between the models.

Reply: Agreed. We elaborate this:

Fig. 8g, 8h shows that the zonal means are noisier than for TNn and TXx. The results look much more complex than the temperature extreme indices in Fig. 6h and 7h. The general effect is that the tropical regions (30ºS-30ºN) are more strongly affected by aerosol injection than by solar dimming. The mid-latitude Rx5day is more effectively changed by stratospheric aerosol injection geoengineering year-round, especially in the Northern Hemisphere. Except for summertime polar areas, solar dimming geoengineering is relatively more effective year-round at high-latitudes, especially in the southern hemisphere. Ferraro et al. (2014) found that the tropical overturning circulation weakens in response to geoengineering with stratospheric sulphate aerosol injection due to radiative heating from the aerosol layer, but geoengineering simulated as a simple reduction in total solar irradiance do not capture this effect. Therefore, a relatively large tropical precipitation perturbation occurs under stratospheric aerosol injection. On the other hand, the meridional distribution of the sulfate aerosols is handled different between the models (as outlined in Section 3.1), which also contributes the noisier Rx5Day pattern showing in Fig. 8d, 8g and 8i. Four of the six models (BNU-ESM, CanESM2, MIROC-ESM and NorESM1-M) analysed in our study use the AOD prescribed to mimic the one-fourth of the 1991 eruption of Mount Pinatubo, but with different AOD meridional distribution, particle effective radii, and standard deviations of their log-normal size distribution (Kashimura et al., 2017). Another two models (GISS-E2-R and HadGEM2-ES) adopt different stratospheric aerosol schemes to simulate the sulfate AOD.

Line 21: 'at high latitudes winter solar dimming ...' How can this be? There is no sunlight, so no SW reduction. < Line 23/24: 'Stratospheric vortex' I doubt that you see this with significant signals in the models even it seems to be a reasonable explanation. E.g. Driscoll et al. (2012) showed that climate model do not represent stratospheric dynamic repose of volcanic eruptions very well. You may show the zonal wind (DJF) and significance of the single models to approve the hypothesis.

Reply: Thanks. We revise this part and deleted the sentence on speculating stratospheric vortex change as following:

The mid-latitude Rx5day is more effectively changed by stratospheric aerosol injection geoengineering year-round, especially in the Northern Hemisphere. Except for summertime polar areas, solar dimming geoengineering is relatively more effective year-round at high-latitudes, especially in the Southern Hemisphere.

Page 24

Line 1 to 6: Does this result it to Jones et al. (2017)?

Reply: No. Jones et al. (2017) found the stratospheric aerosol injection (SAI) applied to the southern hemisphere **only** would enhance tropical cyclone frequency relative to a global SAI application, and vice versa for SAI in the northern hemisphere **only**. Here our study of **global** geoengineering indicates the tropical storms and hurricanes are more effectively moderated in the Northern Hemisphere by global SAI and in the Southern Hemisphere by global solar dimming.

References
Some are missing in the list. Please check.

Reply: Thanks. We add several missing references. Such as Latham (1990), Niemeier et al. (2013), Pitari et al. (2014), Smyth et al. (2017):

Latham, J.: Control of global warming?, Nature, 347, 339–340, 1990.

Niemeier, U., Schmidt, H., Alterskjær, K., and Kristjánsson, J. E.: Solar irradiance reduction via climate engineering: Impact of different techniques on the energy balance and the hydrological cycle, J. Geophys. Res. Atmos., 118, 11905–11917, doi:10.1002/2013JD020445, 2013.

Pitari, G., Aquila, V., Kravitz, B., Robock, A., Watanabe, S., Cionni, I., Luca, N. D., Genova, G. D., Mancini, E., and Tilmes, S.: Stratospheric ozone response to sulfate geoengineering: Results from the Geoengineering Model Intercomparison Project (GeoMIP), J. Geophys. Res.-Atmos., 119, 2629–2653, 2014.

Smyth, J. E., Russotto, R. D., and Storelvmo, T.: Thermodynamic and dynamic responses of the hydrological cycle to solar dimming, Atmos. Chem. Phys., 17, 6439-6453, doi:10.5194/acp-17-6439-2017, 2017.

References

Driscoll, S., Bozzo, A., Gray, L. J., Robock, A., and Stenchikov, G.: Coupled Model Intercom- parison Project 5 (CMIP5) simulations of climate following volcanic eruptions, Journal of Geophysical Research: Atmospheres, 117, doi:10.1029/2012JD017607, 2012.

Jones, A. C. J. M. H., Dunstone, N., Hawcroft, K. E. M. K., and Jones, K. H. A.: Impacts of hemispheric solar geoengineering on tropical cyclone frequency, Nature Communications, 8, 1383, doi:10.1038/s41467-017-01606-0, 2017.

Pitari, G., Aquila, V., Kravitz, B., Robock, A., Watanabe, S., Luca, N. D., Genova, G. D., Mancini, E., Tilmes, S., and Cionni, I.: Stratospheric ozone response to sulfate geoengineering: Results from the Geoengineering Model Intercomparison Project (GeoMIP), Journal of Geophysical Research, 119, 2629–2653, doi:10.1002/2013JD020566, 2013.

Xia, L., Nowack, P. J., Tilmes, S., and Robock, A.: Impacts of stratospheric sulfate geoengineering on tropospheric ozone, Atmospheric Chemistry and Physics, 17, 11 913–11 928, doi:10.5194/acp-17-11913-2017, URL https://www.atmos-chem-phys.net/17/11913/2017/, 2017.

Response to Review of "Extreme temperature and precipitation response to solar dimming and stratospheric aerosol geoengineering" by D. Ji et al.

We first thank the referee for his/her insightful comments, which helped us clarify and greatly improve the paper. In the reply, the referee's comments are in *italics*, our response is in normal and changes to the text are shown in blue.

Anonymous Referee #2

General Comments: In this manuscript, the authors analyzed the extreme values of climate indicators under 2 different solar radiation management scenarios G1 and G4. They took extreme index by ETCCDI and applied it on temperature and precipitation. The authors tried to find the differences and similarities on the global impact of two SRM experiment. And also tried to analysis the differences among the model.

This manuscript is novel and further complete the understanding of SRM. The structure is also well organized. I recommend the manuscript for publication though some of the comments still should be fixed or rephrased.

Specific Comments:

1. The significant regions in Fig. 2c and 4c,f,j need further descriptions on calculation process;

Reply: Yes. We've revised the previous Figure 2 and Figure 4. In our new Figure 1 and Figure 4 (we reorder some paragraph, previous Fig.2 is labelled as Fig. 1 now, please refer to our replies to Referee #1), we show the normalized results. We normalize the values of each grid from the differences of G1-abrupt4xCO2 according to the global average of G1-abrupt4xCO2, same for G4-rcp45. With these normalized results, we present the difference between normalized G1-abrupt4xCO2 and G4-rcp45 instead of the ratio between non-normalized G1-abrupt4xCO2 and G4-rcp45 to avoid large unrealistic values. In Figure 6, 7 and 8, we also show the differences of zonally normalized results in several single figures instead of ratios between non-normalized fields. We define all normalization methods in Section 2: Data and methods as the following:

2.3 Normalization methods

There are large differences in forcing between the G1 solar dimming and G4 stratospheric aerosol injection geoengineering schemes. The mean and extreme climates under the two type geoengineering are quite different as will be shown below. To aid the comparisons, we adopt the following normalization methods to compare spatially relative effectivities between solar dimming and stratospheric aerosol injection.

The normalized global spatial effects of solar dimming or stratospheric aerosol injection are defined as the grid mean difference relative to the global mean difference:

$$< X^{geo} - X^{ref} > = \frac{\overline{X}^{geo}_{grid} - \overline{X}^{ref}_{grid}}{|\overline{X}^{geo}_{global} - \overline{X}^{ref}_{global}|}$$

where the operator <> denotes the normalized grid value, X is TXx, TNn, Rx5day or other climate field, an overbar denotes the average of each grid cell or the global average, the absolute operator || in the denominator of the right term preserves the sign of the geoengineering anomaly. The superscript "geo" represents geoengineering experiments of G1 solar dimming or G4 stratospheric aerosol injection, the superscript "ref" represents the reference experiments of abrupt4×CO2 or rcp45.

To normalize zonal mean difference in the climate extreme indices relative to the global mean difference, we use a similar formula:

$$< X^{geo} - X^{ref} >= \frac{\overline{X}^{geo}_{zonal} - \overline{X}^{ref}_{zonal}}{|\overline{X}^{geo}_{global} - \overline{X}^{ref}_{global}|}$$

where the operator <> denotes the normalized zonal mean, an overbar denotes the zonal or global average, the absolute operator || in the denominator of the right term preserves the sign of the geoengineering anomaly.

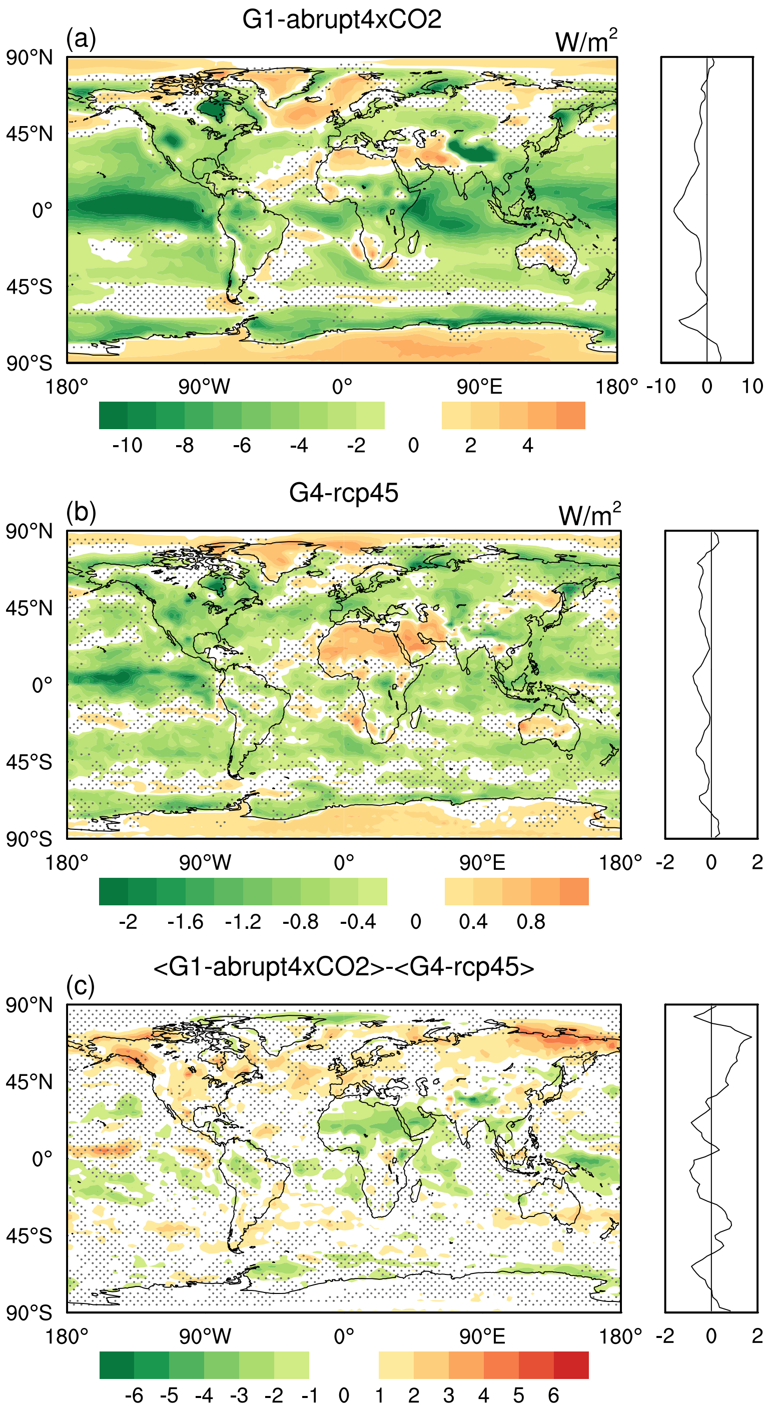

Figure 1: Geographical distributions over the 40-year analysis periods of differences in net radiation flux at TOA between G1-abrupt4×CO2 (top), G4-rcp45 (middle). The bottom panel shows the differences in net radiation flux at TOA between normalized G1-abrupt4×CO2 and G4-rcp45 Stippling indicates regions where fewer than 5 of 6 models agree on the sign of the model response. The right sub-panels show the zonal average of the left sub-panels. Note that all three panels have different scales.

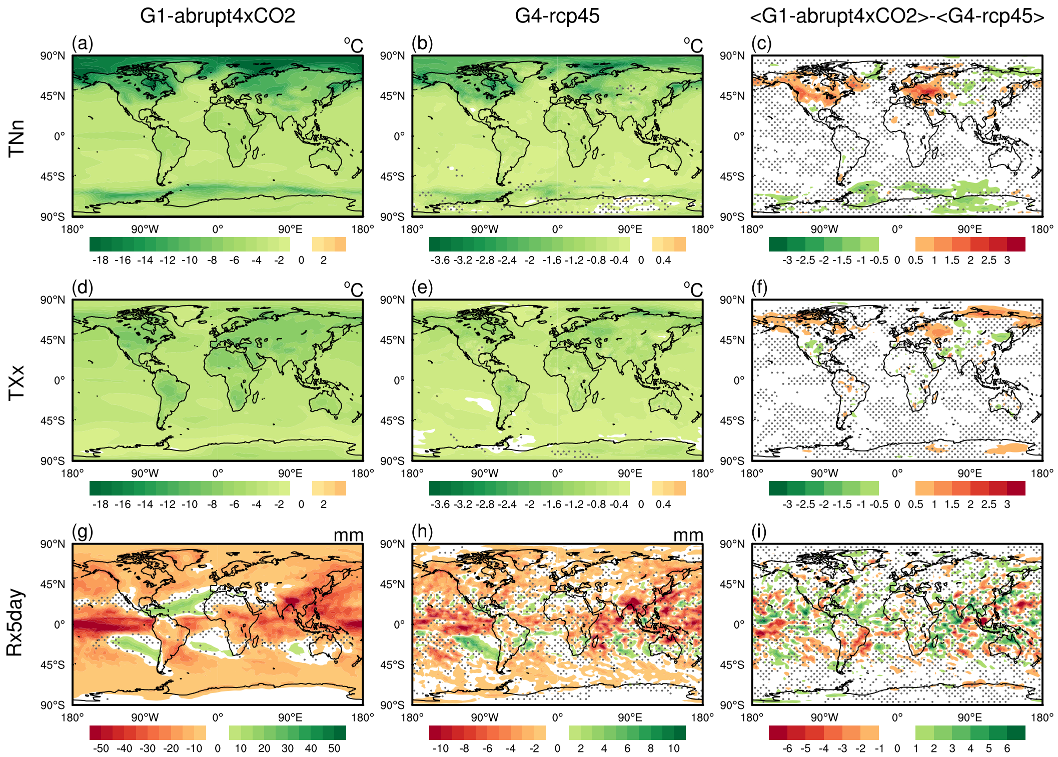

Figure 4: Geographical distributions over the 40-year analysis periods of the differences G1 - abrupt4×CO2 (left column), G4 - rcp45 (middle column), and differences between normalized G1 - abrupt4×CO2 and G4 - rcp45 (right column) for the extreme indices TNn (top row), TXx (middle row), and Rx5day (bottom row). Stippling indicates regions where fewer than 5 of 6 models agree on the sign of the model response. Note that panels have different colour scales.

2. The uncertainty reason present on abstract may not be proper here. Rephrase the word may be better.

Reply: Thanks. We revise the abstract as the following:

We examine extreme temperature and precipitation under two potential geoengineering methods forming part of the Geoengineering Model Intercomparison Project (GeoMIP). The solar dimming experiment G1 is designed to completely offset the global mean radiative forcing due to a CO_2-quadrupling experiment (abrupt4×CO2), while in GeoMIP experiment G4, the radiative forcing due to the representative concentration pathway 4.5 (RCP4.5) scenario is partly offset by a simulated layer of aerosols in the stratosphere. Both G1 and G4 geoengineering simulations lead to lower minimum temperatures (TNn) at higher latitudes, and on land primarily through feedback effects involving high latitude processes such as snow cover, sea ice and soil moisture. There is larger cooling of TNn and maximum temperatures (TXx) over land compared with oceans, and the land-sea cooling contrast is larger for TXx than TNn. Maximum 5-day precipitation (Rx5day) increases over subtropical oceans, whereas warm spells decrease markedly in the tropics, and the number of consecutive dry days decreases in most deserts. The precipitation during the tropical cyclone (hurricane) seasons becomes less intense, whilst the remainder of the year becomes wetter. Stratospheric aerosol injection is more effective than solar dimming in moderating extreme precipitation (and flooding). Despite the magnitude of the radiative forcing applied in G1 being ~7.7 times larger than in G4, and differences in the aerosol chemistry and transport schemes amongst the models, the two types of geoengineering show similar spatial patterns in normalized differences of extreme temperatures changes. Large differences mainly occur at northern high latitudes, where stratospheric aerosol injection more effectively reduces TNn and TXx. While the pattern of normalized differences of extreme precipitation is more complex than that of extreme temperatures, generally stratospheric aerosol injection is more effective in reducing tropical Rx5day, while solar dimming is more effective over extra-tropical regions.

3. On Page 15, Line 1-6, this paragraph are not linked so well with the context. There are also no further analysis on the daily rain types. Further explanation and graphs would be better.

Reply: Thanks. As this is at the end of "3.4 Spatial Response in Extremes", and the tropical precipitation change constitutes a large percentage of global precipitation change, therefore we would like to address how the tropical precipitation change in response to G1 solar dimming and G4 stratospheric aerosol injection in different major rain types. To make it clear, we add the following sentence:

As the tropical extreme precipitation change constitutes a large percentage of global extreme precipitation change in response to two type geoengineering schemes (Fig. 4g, 4h), it is interesting to know how the G1 solar dimming and G4 stratospheric aerosol injection affect major rain types in tropical regions.

Minor comments:

1. P2 L18: Missed ref. Lathan et al. 2. P3 L12: Missed ref. Niemeier et al.

Reply: Thanks. We add missing references, such as Latham (1990), Niemeier et al. (2013), Pitari et al. (2014), Smyth et al. (2017):

Latham, J.: Control of global warming?, Nature, 347, 339–340, 1990.

Niemeier, U., Schmidt, H., Alterskjær, K., and Kristjánsson, J. E.: Solar irradiance reduction via climate engineering: Impact of different techniques on the energy balance and the hydrological cycle, J. Geophys. Res. Atmos., 118, 11905–11917, doi:10.1002/2013JD020445, 2013.

Pitari, G., Aquila, V., Kravitz, B., Robock, A., Watanabe, S., Cionni, I., Luca, N. D., Genova, G. D., Mancini, E., and Tilmes, S.: Stratospheric ozone response to sulfate geoengineering: Results from the Geoengineering Model Intercomparison Project (GeoMIP), J. Geophys. Res.-Atmos., 119, 2629–2653, 2014.

Smyth, J. E., Russotto, R. D., and Storelvmo, T.: Thermodynamic and dynamic responses of the hydrological cycle to solar dimming, Atmos. Chem. Phys., 17, 6439-6453, doi:10.5194/acp-17-6439-2017, 2017.

3. P5 L1: The estimate of CSDI and WSDI is applied on ensemble mean temperature or mean CSDI/WSDI?

Reply: The CSDI and WSDI are calculated for each model firstly, then equal weight is given to each model before calculating multi-model ensemble mean. We clarify this point in "Data and Methods" as following:

Equal weight is given to each model in the analysis, and climate extreme indices are calculated for each model before multi-model ensemble averaging is done.

4. P8 L24-27: It is not clear for me about the relations between different models and the geoengineering impact. Further expression would be better.

Reply: Yes, Thanks for this comment. In the revised manuscript we emphasize the differences between G1 solar dimming and G4 stratospheric aerosol injection, and how each model implements the G4 experiment.

In the "Introduction" section, we add previous studies discussing the differences of the two type geoengineering schemes:

Both methods would cool Earth's surface by reducing sunlight reaching the surface, either by aerosols reflecting sunlight or by artificially reducing the solar constant in climate models. The injected stratospheric aerosols under G4 not only scatter shortwave radiation, also absorb near infrared and longer wavelengths (Lohmann and Feichter, 2005). The differences between stratospheric aerosol injection and solar dimming are influenced strongly by the absorption of longwave radiation by aerosols, this atmospheric heating imbalance could further stabilize the troposphere and lead to stronger precipitation reduction under stratospheric aerosol injection than under solar dimming (Niemeier et al., 2013). That there can be a difference in the mean climate response in reduced solar constant and increased stratospheric sulphate aerosols has been shown (Yu et al., 2015; Niemeier et al., 2013; Ferraro et al., 2014) and we expect that this will also be evident in the temperature and precipitation extremes.

In the "Results" section 3.1, we add the following to show the impacts of the two type geoengineering schemes on TOA net radiation flux:

The forcing of the G1 solar dimming and G4 stratospheric aerosol injection experiments are quite different, there can be a difference in the mean and extreme climate responses. The multi-model ensemble mean net radiation flux at the top of atmosphere (TOA) is 2.76 Wm^{-2} and 0.004 Wm^{-2} for the abrupt×4CO2 and G1 experiments, and 1.63 Wm^{-2} and 1.27 Wm^{-2} for the rcp45 and G4 experiments during their 40-year analysis periods. Therefore, the G1 solar dimming and G4 stratospheric aerosol injection exert a reduction of 2.76 Wm^{-2} and 0.36 Wm^{-2} for net radiation fluxes at TOA respectively. The differences of mean net radiation flux at TOA over land and ocean between two geoengineering experiments and their reference experiments are show in Table 3. Although the ratio between the global temporally averaged net radiation flux reductions at TOA is a factor of ~7.7, the spatial distribution of net radiation flux changes for the G1 and G4 ensemble means are quite similar, especially the positive TOA net radiation over Greenland, Antarctica, North Africa and West Asia, and the negative TOA net radiation over North America, Central Europe and tropical ocean basins (Figure 1). The entire ensemble shows a large and consistent positive TOA net radiation east of Greenland in the North Atlantic under G1 solar dimming (Figure 1a), the region associated with the overturning part of the Atlantic meridional circulation (AMOC), and which under the G1 forcing was shown to be strongly affected by changes in radiative forcing and air/ocean heat exchange (Hong et al., 2017). However, differences are clearer when we investigate the spatial pattern of normalized effects exerted by the two SRM experiments, although most regions have differences close to zero for normalized solar dimming and stratospheric aerosol geoengineering effects on TOA net radiation (Figure 1c). The G4 stratospheric aerosol injection geoengineering introduces a more effective reduction in TOA net radiation over the Northern Hemisphere, especially over the high-latitude continents, such as northern North America, Siberia and some regions of western Europe. The G1 solar dimming geoengineering introduces a more effective reduction in TOA net radiation over North Africa, northern South America, the Indian Ocean and tropical Western Pacific. In contrast, many other equatorial regions, the Southern Ocean and the Intertropical and South Pacific Convergence Zones display small differences between normalized solar dimming and stratospheric aerosol injection effects.

The G1 solar dimming assumes global uniform solar reduction, while under G4 sulphate aerosols are handled differently among the participating models. GISS-E2-R and HadGEM2-ES adopt stratospheric aerosol schemes to simulate the sulfate aerosol optical depth (AOD), BNU-ESM and MIROC-ESM use the prescribed meridional distribution of AOD recommended by the GeoMIP protocol, CanESM2 specifies uniform sulfate AOD (Kashimura et al., 2017). NorESM1-M specifies the AOD and effective radius which were calculated in previous simulations with the aerosol microphysical model ECHAM5-HAM (Niemeier et al., 2011, Niemeier and Timmreck, 2015). Although a prescribed AOD can be set, difference in assumed particle size for the stratospheric sulfate aerosols (Pierce et al., 2010) and the warming effects of stratospheric aerosol (Pitari et al., 2014) cause difference in the SRM forcing.

In "Results" section 3.2, we add following to show impacts of two type geoengineering schemes on mean climate states:

The G1 solar dimming and G4 stratospheric aerosol injection geoengineering greatly affected the mean climate states. The annual mean surface air temperatures are 291.0 K and 286.7 K for abrupt4×CO2 and G1 experiments, 288.8 K and 288.3 K for rcp45 and G4 experiments respectively during their 40-year analysis periods. The global hydrological strength is likewise reduced; the annual mean precipitation totals are 1125.8 mm and 1026.9 mm for abrupt4×CO2 and G1 experiments, 1098.4 mm and 1084.3 mm for rcp45 and G4 experiments (Table 3).

5. P12 L2: May be I got missed but I'm not sure what the 'case' indicate.

Reply: In our previous manuscript, the 'case' means the extreme precipitation scales with mean temperature. In the revised manuscript, we largely revise this paragraph as following:

If relative humidity and atmospheric circulation remain relatively unchanged, then intense precipitation amount is governed by total precipitable water in the atmosphere, which the Clausius–Clapeyron relation says scales with mean temperatures (Allen and Ingram, 2002). The global mean precipitation decreases 2.1±0.4% per Kelvin in response to G1 solar dimming, and 2.7±1.0% per Kelvin in response to G4 stratospheric aerosol injection. The GISS-E2-R model contributes a relatively large portion to the spread of scaling between mean precipitation and temperature with a value of 4.5% per Kelvin for G4. If excluding the GISS-E2-R model, the global mean precipitation decreases 2.0±0.4% per Kelvin in response to G1 solar dimming, and 2.3±0.5% per Kelvin in response to G4 stratospheric aerosol injection. The scaling between mean precipitation and mean temperature under G1 and G4 is smaller than 3.4% precipitation change per Kelvin estimated from other coupled models under long-term equilibrium climate in response to doubling CO_2 (Allen and Ingram, 2002). The global mean Rx5day decreases 3.4±1.0% per Kelvin in response to G1 solar dimming, and 4.3±2.6% per Kelvin in response to G4 stratospheric aerosol injection. GISS-E2-R gives global mean Rx5day decreases 9.5% per Kelvin for G4. If excluding GISS-E2-R model, the global mean Rx5day decreases 3.4±1.1% per Kelvin in response to G1 solar dimming, and 3.3±0.6% per Kelvin in response to G4 stratospheric aerosol injection. The scaling of mean precipitation and mean temperature is expected to be much less than the 6.5% per Kelvin implied by the Clausius–Clapeyron relation, as the global-mean precipitation is primarily constrained by the availability of energy not moisture (Pall et al., 2007). The scaling of Rx5day and mean temperature under G1 and G4 is close to, but still weaker than the Clausius–Clapeyron relation, probably because Rx5day is not really an index of the heaviest rainfall events that are expected to be constrained by the Clausius–Clapeyron relation. The Clausius–Clapeyron relation implies the same scaling of extreme precipitation and mean temperatures under both G1 and G4 experiments, which is the case here for five of six models, but not the GISS-E2-R model.

6. P13 L28: Eastern China in Fig4 seems no special around the globe, this part may need further explanation.

Reply: We deleted this sentence. It's more likely a regional feature which is usually not very well represented in the models as suggested by Referee #1.

7. P14 L10-13: The reduction of Rx5day is whether a result from Curry et al., 2014 or from the paper result? Further explanation would be better.

Reply: Here we mean the results from the previous study by Curry et al. (2014). In our study, we also find the reduction of Rx5day under solar dimming and stratospheric aerosol injection geoengineering schemes. Please refer to the revised sentences following this line:

The ensemble means show that Rx5day is strongly reduced over equatorial regions, especially in the equatorial Pacific and southern flank of the Tibetan Plateau (Fig. 4g, 4h). This is due to increased atmospheric stability and suppression of convection under geoengineering (Bala et al.,2008).

8. P15 L1-6: The paragraph may not fully link with the context and there is no graphs or tables to support the statistics.

Reply: The numbers given are from simple calculations of the model precipitation output. We could have put them in a table but it seemed more concise to simply give the statistics as a sentence. The context comes because we are discussing Rx5day throughout the paragraph, and in particular tropical and monsoon rains (that is heavy rain).

Extreme temperature and precipitation response to solar dimming and stratospheric aerosol geoengineering

Duoying Ji[1], Songsong Fang[1], Charles L. Curry[2,3], Hiroki Kashimura[4], Shingo Watanabe[5], Jason N. S. Cole[6], Andrew Lenton[7], Helene Muri[8,9], Ben Kravitz[10] and John C. Moore[1,11,12]

[1]College of Global Change and Earth System Science, Beijing Normal University, Beijing 100875, China
[2]School of Earth and Ocean Sciences, University of Victoria, Victoria, British Columbia, Canada
[3]Pacific Climate Impacts Consortium, University of Victoria, Victoria, British Columbia, Canada
[4]Department of Planetology/Center for Planetary Science, Kobe University, Kobe, Japan
[5]Japan Agency for Marine-Earth Science and Technology, Yokohama, Japan.
[6]Canadian Centre for Climate Modelling and Analysis, Environment and Climate Change Canada, Victoria, British Columbia, Canada
[7]Oceans and Atmosphere, Hobart, Tasmania, Australia
[8]Department of Geosciences, University of Oslo, Oslo, Norway
[9]Department of Energy and Process Engineering, Norwegian University of Science and Technology, Trondheim, Norway
[10]Atmospheric Sciences and Global Change Division, Pacific Northwest National Laboratory, Washington, USA
[11]Arctic Centre, University of Lapland, P.O. Box 122, 96101 Rovaniemi, Finland
[12]CAS Center for Excellence in Tibetan Plateau Earth Sciences, Beijing 100101, China

Correspondence to: John C. Moore (john.moore.bnu@gmail.com)

Abstract.

We examine extreme temperature and precipitation under two potential geoengineering methods forming part of the Geoengineering Model Intercomparison Project (GeoMIP). The solar dimming experiment G1 is designed to completely offset the global mean radiative forcing due to a CO_2-quadrupling experiment (abrupt4×CO2), while in GeoMIP experiment G4, the radiative forcing due to the representative concentration pathway 4.5 (RCP4.5) scenario is partly offset by a simulated layer of aerosols in the stratosphere. Both G1 and G4 geoengineering simulations lead to lower minimum temperatures (TNn) at higher latitudes, and on land primarily through feedback effects involving high latitude processes such as snow cover, sea ice and soil moisture. There is larger cooling of TNn and maximum temperatures (TXx) over land compared with oceans, and the land-sea cooling contrast is larger for TXx than TNn. Maximum 5-day precipitation (Rx5day) increases over subtropical oceans, whereas warm spells decrease markedly in the tropics, and the number of consecutive dry days decreases in most deserts. The precipitation during the tropical cyclone (hurricane) seasons becomes less intense, whilst the remainder of the year becomes wetter. Stratospheric aerosol injection is more effective than solar dimming in moderating extreme precipitation (and flooding). Despite the magnitude of the radiative forcing applied in G1 being ~7.7 times larger than in G4, and differences in the aerosol chemistry and transport schemes amongst the models, the two types of geoengineering show similar spatial patterns in normalized differences of extreme temperatures changes. Large differences mainly occur at northern high latitudes, where stratospheric aerosol injection more effectively reduces TNn and TXx. While the pattern of normalized differences of extreme precipitation is more complex than that of extreme temperatures, generally stratospheric aerosol injection is more effective in reducing tropical Rx5day, while solar dimming is more effective over extra-tropical regions.

1 Introduction

Global atmospheric greenhouse gas (GHG) concentrations continue to increase due to slow progress in reducing net GHG emissions in the industrialized world. Even if countries with existing commitments reduce emissions to meet their national goals (or aspirational targets under the 2015 Paris Agreement), this may not be sufficient to avoid dangerous or irreversible climate change (Sanderson et al., 2016). Climate engineering is increasingly being discussed as a means to lessen or ameliorate the effects of global warming. In particular, Solar Radiation Management (SRM), the artificial reduction of incoming solar radiation has been increasingly studied: examples include mirrors in space (Mautner, 1989), stratospheric aerosol injection (e.g., Budyko, 1977; Crutzen, 2006) or marine cloud brightening (e.g., Latham, 1990). Scientific investigation of SRM has made use of several different climate models examining various degrees of SRM and greenhouse gas forcing (e.g., Bala et al., 2008; Irvine et al., 2011; Schmidt et al., 2012). While gross features of (for example) global temperature patterns under SRM appear robust, more subtle climate indices require standardized experimental design. Kravitz et al. (2011, 2013c) defined a set of numerical SRM experiments under the Geoengineering Model Intercomparison Project (GeoMIP), comprising solar dimming experiments (G1 and G2), stratospheric aerosol injection simulations (G3 and G4) and marine cloud brightening experiments (G4cdnc, G4sea-salt).

The mean climate response under G1 and G2 of diverse climate variables, e.g. temperature, precipitation, sea level pressure has been well described (e.g., Schmidt et al., 2012; Kravitz et al., 2013b; Tilmes et al., 2013; Jones et al., 2013). Curry et al. (2014) drew attention to the changes in temperature and precipitation extremes in models running the reduced solar radiation G1 experiment, and Aswathy et al. (2015) examined extremes under G3 and G3-SSCE (marine cloud brightening by sea salt emission, modelled after GeoMIP experiment G3). Dagon and Schrag (2017) showed that solar geoengineering mitigates extreme heat events from greenhouse warming, though the regional response is variable in part due to varying soil moisture content: soils dry out over the course of the summer as daily maximum temperature increases, and this relationship is strengthened under solar geoengineering. These are the only dedicated analyses of climate model extreme indices under geoengineering to date.

This paper will provide a first look at the difference in the extremes of temperature and precipitation between two geoengineering methods: G1 (solar dimming) and G4 (stratospheric aerosol injection) experiments. Both methods would cool Earth's surface by reducing sunlight reaching the surface, either by aerosols reflecting sunlight or by artificially reducing the solar constant in climate models. The injected stratospheric aerosols under G4 not only scatter shortwave radiation, also absorb near infrared and longer wavelengths radiation (Lohmann and Feichter, 2005). The differences between stratospheric aerosol injection and solar dimming are influenced strongly by the absorption of longwave radiation by aerosols; this atmospheric heating imbalance could further stabilize the troposphere and lead to stronger precipitation reduction under stratospheric aerosol injection than under solar dimming (Niemeier et al., 2013). That there can be a difference in the mean climate response in reduced solar constant and increased stratospheric sulphate aerosols has been shown previously (Yu et al., 2015; Niemeier et al., 2013; Ferraro et al., 2014) and we expect that this will also be evident in the temperature and precipitation extremes. We perform analyses on daily output from GeoMIP models that have completed both G1 and G4, which is a limited subset of models with several excluded from these analyses because only monthly resolution output was saved. We take the results from G1 relative to its corresponding CMIP5 experiment, abrupt4×CO2 to examine impacts of solar dimming, and take the results from G4 relative to rcp45 (the simulations forced by the RCP4.5 scenario) as the impact of stratospheric aerosol injection. The paper is organized as follows: The multimodel ensembles and the definitions of indices are briefly described in Section 2. The probability density functions of monthly mean temperature and precipitation and the results are given in Section 3, along with global mean time series and spatial and seasonal differences of the extreme climate indices in the two SRM experiments. Finally, and a summary of the main findings and conclusion are given in Section 4.

2 Data and Methods

2.1 GeoMIP experiments

G1 simulates balancing the GHG forcing from the CMIP5 experiment abrupt4×CO2 (instantly quadrupled CO_2 relative to pre-industrial levels) by decreasing solar irradiance. The G1 experiment runs for 50 years beginning from the control run (the piControl scenario; Taylor et al., 2012). The globally averaged top of atmosphere (TOA) radiation differences between G1 and piControl are no more than 0.1 Wm^{-2} (Kravitz et al., 2011). The G1 results can also be naturally compared with results from the abrupt4×CO2 simulation itself, which most model groups have performed (Taylor et al., 2012).

G4 is based on the RCP4.5 future climate scenario (hereafter "rcp45", Meinshausen et al., 2011; Taylor et al., 2012), with additional injection of SO_2 into the tropical lower stratosphere at a rate of 5 Tg per year from the year 2020. The G4 experiments do not specify any specific treatment of chemical or physical properties, so inter-model differences are expected to be larger than in G1 simply from differences in the implementation of the stratospheric aerosol injection (Kravitz et al., 2011; Yu et al., 2015). The stratospheric aerosol injection experiment, G4, is a much smaller signal with respect to its reference under the mild GHG forcing specified by RCP4.5 than the G1 experiment with respect to its reference abrupt4×CO2. The global temporally averaged forcing of the G1 solar dimming experiment ranges from -9.6 to -6.4 Wm^{-2}, and the G4 stratospheric aerosol injection experiment ranges from −3.6 to −1.6 Wm^{-2}, depending on the model (Schmidt et al., 2012; Kashimura et al., 2017).

We analyze the daily output from six Earth system models, which completed both the G1 and G4 experiments (Table 1). In order to compare the impacts of the two SRM methods, we also made use of the corresponding outputs from piControl, abrupt4×CO2, and rcp45. We exclude the first decade following the large increase in forcing in common with other authors (Schmidt et al., 2012; Curry et al. 2014), and base our analysis on 40 years of data. All G1 and abrupt4×CO2 simulations are analyzed over a common period of simulation years 11 to 50, and the G4 and rcp45 simulations are analyzed from year 2030 to 2069. Equal weight is given to each model in the analysis, and climate extreme indices are calculated for each model before multi-model ensemble averaging is done.

2.2 Climate extreme indices

Here we use the climate indices defined by the Expert Team on Climate Change Detection and Indices (ETCCDI) (Zhang et al., 2011) to provide a comprehensive overview of temperature and precipitation changes based on daily output of multi-models in GeoMIP and the Climate Model Intercomparison Project Phase 5 (CMIP5; Taylor et al., 2012). These indices have been widely used previously, both for observed weather (Donat et al., 2013) and model output (Tebaldi et al., 2006; Orlowsky and Seneviratne, 2012; Seneviratne et al., 2012) with Curry et al. (2014) using them for G1, Aswathy et al (2015) for G3, and Sillmann et al. (2013b) for CMIP5 models running the RCP scenarios.

We use six indices to describe temperature and precipitation extremes (Table 2), based on the daily output of surface air temperature and precipitation (tasmin, tasmax, pr). TXx and TNn are the maximum daily maximum and minimum daily minimum, respectively, of 2-m air temperature. These are absolute indices, representing the hottest or coldest day of a year or a month. The duration indices CSDI and WSDI are the longest number of consecutive days below (exceeding) the 10th (90th) percentiles of daily minimum (maximum) temperatures (Table 2) calculated from piControl and indicate the length of cold spells and warm spells. The precipitation index Rx5day, the maximum 5-day precipitation sum in a month or year, can be taken as a rough indicator of increased flood probability (Frich et al., 2002). CDD is the maximum number of consecutive dry days with precipitation < 1 mm in a year, and is often referred to as a drought indicator.

All model output fields were re-sampled to a median model grid resolution of 144×90 (2.5° longitude × 2° latitude), which corresponds to the grid of the GISS-E2-R model. Following Curry et al. (2014) we adopted a first-order conservative remapping algorithm for non-integer variables (TXx, TNn, and Rx5day), (Jones, 1999), and nearest-neighbour interpolation for integer variables (CSDI, WSDI, and CDD).

2.3 Normalization methods

There are large differences in forcing between the G1 solar dimming and G4 stratospheric aerosol injection geoengineering schemes. The mean and extreme climates under the two types of geoengineering are quite different as will be shown below. To aid the comparisons, we adopt the following normalization methods to compare spatially relative effectivities between solar dimming and stratospheric aerosol injection.

The normalized global spatial effects of solar dimming or stratospheric aerosol injection are defined as the grid mean difference relative to the global mean difference:

$$< \mathrm{X}^{\mathrm{geo}} - \mathrm{X}^{\mathrm{ref}} >= \frac{\overline{\mathrm{X}}^{\mathrm{geo}}_{\mathrm{grid}} - \overline{\mathrm{X}}^{\mathrm{ref}}_{\mathrm{grid}}}{|\overline{\mathrm{X}}^{\mathrm{geo}}_{\mathrm{global}} - \overline{\mathrm{X}}^{\mathrm{ref}}_{\mathrm{global}}|}$$

where the operator <> denotes the normalized grid value, X is TXx, TNn, Rx5day or other climate field, an overbar denotes the average of each grid cell or the global average, the absolute operator || in the denominator of the right term preserves the sign of the geoengineering anomaly. The superscript "geo" represents geoengineering experiments of G1 solar dimming or G4 stratospheric aerosol injection, the superscript "ref" represents the reference experiments of abrupt4×CO2 or rcp45.

To normalize zonal mean difference in the climate extreme indices relative to the global mean difference, we use a similar formula:

$$< \mathrm{X}^{\mathrm{geo}} - \mathrm{X}^{\mathrm{ref}} >= \frac{\overline{\mathrm{X}}^{\mathrm{geo}}_{\mathrm{zonal}} - \overline{\mathrm{X}}^{\mathrm{ref}}_{\mathrm{zonal}}}{|\overline{\mathrm{X}}^{\mathrm{geo}}_{\mathrm{global}} - \overline{\mathrm{X}}^{\mathrm{ref}}_{\mathrm{global}}|}$$

where the operator <> denotes the normalized zonal mean, an overbar denotes the zonal or global average, the absolute operator || in the denominator of the right term preserves the sign of the geoengineering anomaly.

3 Results

When discussing changes in climate variables the choice of reference scenario is important, though somewhat arbitrary. Curry et al. (2014) chose piControl as the reference for their study of G1, but here we choose abrupt4×CO2 as the reference for G1 and rcp45 as the reference for G4. Our motivation for doing this is that because a return to pre-industrial era is not proposed or even likely to be desirable given the enormous quantities of GHG that would need to be removed from the climate system, in reality we will have to choose between either a world with GHG forcing, or with GHG forcing plus geoengineering. Atmospheric CO_2 concentrations equal those in abrupt4×CO2 would be reached by about the year 2100 under business-as-usual scenarios like RCP8.5.

3.1 TOA net radiation

The forcing of the G1 solar dimming and G4 stratospheric aerosol injection experiments are quite different, there can be a difference in the mean and extreme climate responses. The multi-model ensemble mean net radiation flux at the top of atmosphere (TOA) is 2.76 Wm^{-2} and 0.004 Wm^{-2} for the abrupt×4CO2 and G1 experiments, and 1.63 Wm^{-2} and 1.27 Wm^{-2} for the rcp45 and G4 experiments during their 40-year analysis periods. Therefore, the G1 solar dimming and G4 stratospheric aerosol injection exert a reduction of 2.76 Wm^{-2} and 0.36 Wm^{-2} for net radiation fluxes at TOA respectively. The differences of mean net radiation flux at TOA over land and ocean between two geoengineering experiments and their reference experiments are show in Table 3. Although the ratio between the global temporally averaged net radiation flux reductions at TOA is a factor of ~7.7, the spatial distribution of net radiation flux changes for the G1 and G4 ensemble means are quite similar, especially the positive TOA net radiation over Greenland, Antarctica, North Africa and West Asia, and the negative TOA net radiation over North America, Central Europe and tropical ocean basins (Figure 1). The entire ensemble shows a large and consistent positive TOA net radiation east of Greenland in the North Atlantic under G1 solar dimming (Figure 1a), the region associated with the overturning part of the Atlantic meridional circulation (AMOC), and which under the G1 forcing was shown to be strongly affected by changes in radiative forcing and air/ocean heat exchange (Hong et al., 2017). However, differences are clearer when we investigate the spatial pattern of normalized effects exerted by the two SRM experiments, although most regions have differences close to zero for normalized solar dimming and stratospheric aerosol geoengineering effects on TOA net radiation (Figure 1c). The G4 stratospheric aerosol injection geoengineering introduces a more effective reduction in TOA net radiation over the Northern Hemisphere, especially over the high-latitude continents, such as northern North America, Siberia and some regions of western Europe. The G1 solar dimming geoengineering introduces a more effective reduction in TOA net radiation over North Africa, northern South America, the Indian Ocean and tropical Western Pacific. In contrast, many other equatorial regions, the Southern Ocean and the Intertropical and South Pacific Convergence Zones display small differences between normalized solar dimming and stratospheric aerosol injection effects.

The models show more consistent responses under G1 solar dimming then under G4 stratospheric aerosol injection, which is probably due to smaller signal-to-noise ratios under G4. The models are inconsistent under both G1 and G4 over the Southern Ocean around Antarctica, where CMIP5 models also show large uncertainties in cloud radiative effects (Stocker et al. 2013). These results suggest that solar dimming and stratospheric aerosol injection geoengineering forcing may affect clouds differently in some models: low level clouds are important for radiative surface fluxes in the North Atlantic where differences between G1 and G4 are positive, while higher clouds are more important in the deep tropical convection regions where differences are weakly negative. It is also possible that the different mean climate states between G1 and G4, and surface albedo changes due to sea ice and snow cover are responsible for the large differences in net radiation flux in the coastal Antarctic seas, and the more modest differences seen in the North Atlantic and Barents Sea along with Alaska and eastern Siberia.

In addition to different mean climate states and cloud responses, there are numerous sources of inter-model differences in response to solar dimming and stratospheric aerosol injection geoengineering. The G1 solar dimming assumes global uniform solar reduction, while under G4 sulphate aerosols are handled differently among the participating models. GISS-E2-R and HadGEM2-ES adopt stratospheric aerosol schemes to simulate the sulphate aerosol optical depth (AOD), BNU-ESM and MIROC-ESM use the prescribed meridional distribution of AOD recommended by the GeoMIP protocol, CanESM2 specifies the uniform sulphate AOD (Kashimura et al., 2017). NorESM1-M specifies the AOD and effective radius which were calculated in previous simulations with the aerosol microphysical model ECHAM5-HAM (Niemeier et al., 2011; Niemeier and Timmreck, 2015). Although a prescribed AOD can be set, difference in assumed particle size for the stratospheric sulphate aerosols (Pierce et al., 2010) and the warming effects of stratospheric aerosol (Pitari et al., 2014) cause difference in the SRM forcing.

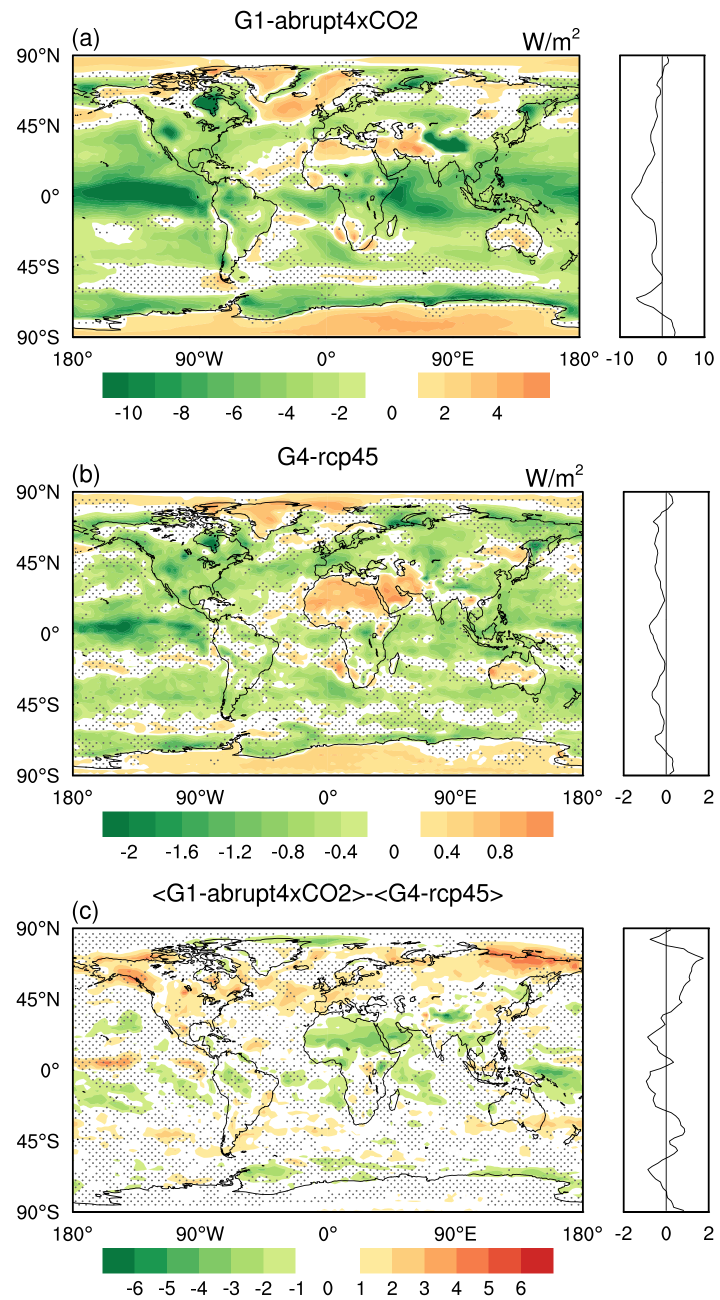

Figure 1: Geographical distributions over the 40-year analysis periods of differences in net radiation flux at TOA between G1-abrupt4×CO2 (top), G4-rcp45 (middle). The bottom panel shows the differences in net radiation flux at TOA between normalized G1-abrupt4×CO2 and G4-rcp45 Stippling indicates regions where fewer than 5 of 6 models agree on the sign of the model response. The right sub-panels show the zonal average of the left sub-panels. Note that all three panels have different scales.

3.2 Probability distributions of monthly temperature and precipitation

The G1 solar dimming and G4 stratospheric aerosol injection geoengineering greatly affected the mean climate states. The annual mean surface air temperatures are 291.0 K and 286.7 K for abrupt4×CO2 and G1 experiments, 288.8 K and 288.3 K for rcp45 and G4 experiments respectively during their 40-year analysis periods. The global hydrological cycle strength is likewise reduced; the annual mean precipitation totals are 1125.8 mm and 1026.9 mm for abrupt4×CO2 and G1 experiments, 1098.4 mm and 1084.3 mm for rcp45 and G4 experiments (Table 3).

We computed the probability density functions (PDFs) of temperature and precipitation for each model and average all models thereafter to get a general idea of the changes in the two geoengineering experiments (G1 and G4) compared to their baseline experiments (abrupt4×CO2 and rcp45). We first calculated the standardized monthly anomalies of monthly mean surface temperature in abrupt4×CO2 and rcp45 at every grid point in each model, i.e.

$$\tau_m^{ref} = (T_m^{ref} - \overline{T}_m^{ref})/\sigma_{T_m}^{ref}$$

where an overbar denotes the means of each month of the year calculated for the 11th to 50th years of the simulations and $\sigma_{T_m}^{ref}$ is the similarly calculated standard deviation for month m in the reference experiment, abrupt4×CO2 or rcp45. Next, we computed the monthly anomalies in G1 and G4 relative to the reference mean and standard deviation, i.e.

$$\tau_m^{geo} = (T_m^{geo} - \overline{T}_m^{ref})/\sigma_{T_m}^{ref}$$

The same algorithm was used to generate PDFs of precipitation. The multi-model mean PDFs use equal weights for each model. The results are shown in Figure 2. The PDFs for G1 and abrupt4×CO2 differ from those presented by Curry et al. (2014) as expected, due to the different choice of reference simulation. Curry et al. (2014) use the piControl as the reference experiment and compare the PDFs of G1 with piControl, which suggests temperature and precipitation perturbations that occur under abrupt4×CO2 are all reduced to near-piControl values by G1 solar dimming geoengineering. In our study, we choose abrupt4×CO2 as the reference for G1, and rcp45 as the reference for G4, as we aim to investigate how the global mean and extreme temperatures and precipitation events may be ameliorated by G1 solar dimming and G4 stratospheric aerosol injection geoengineering compared to global warming.

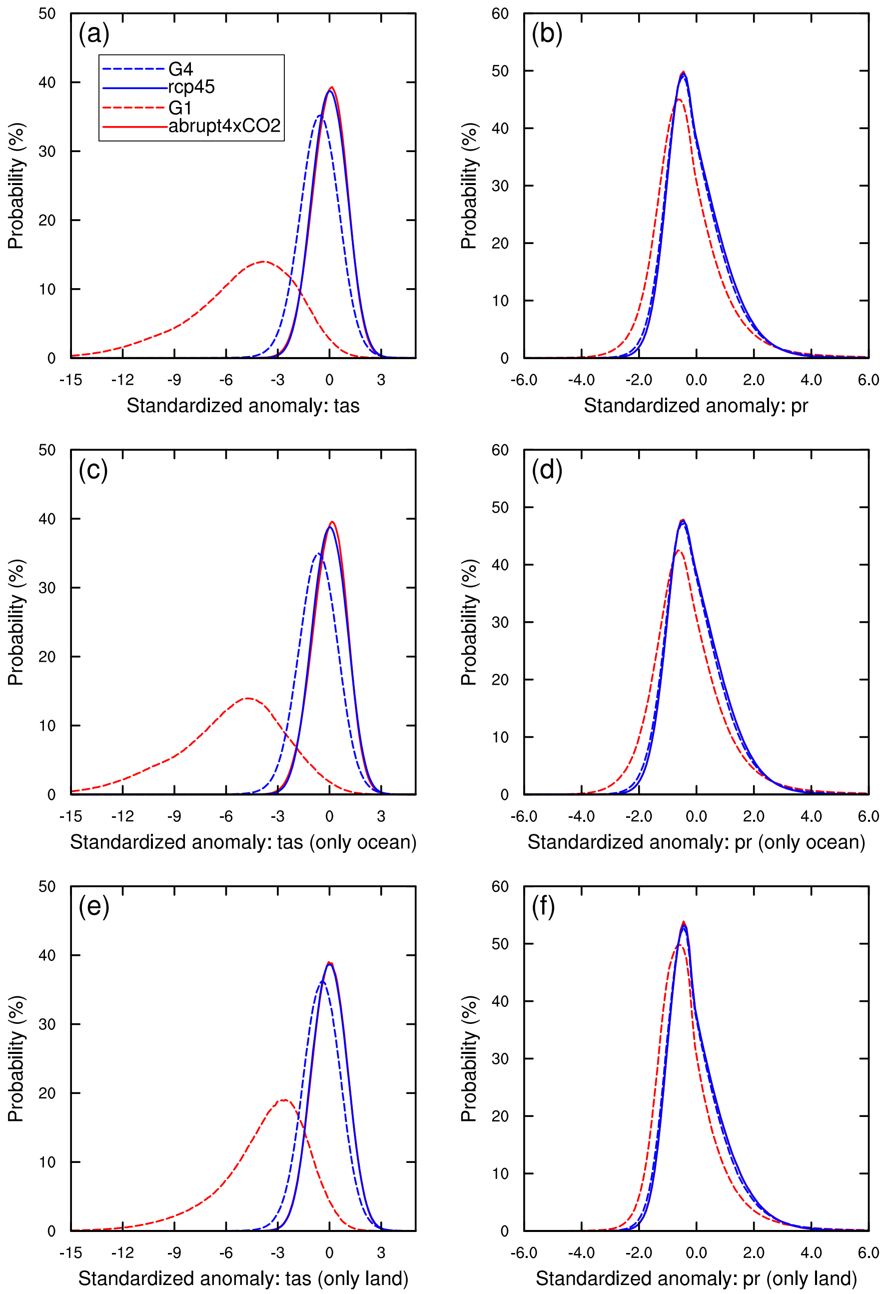

Figure 2: Probability density distributions, normalized to 100%, of standardized monthly mean anomalies for the model ensemble average for four experiments: abrupt4×CO2 (solid red line), G1 (dashed red line), rcp45 (solid blue line), and G4 (dashed blue line). The PDFs of surface air temperature are shown in the left-hand panels, precipitation in the right-hand panels. Upper panels show global results, middle panels ocean-only, and lower panels land-only. *tas* denotes surface air temperature, while *pr* denotes precipitation.

The PDFs of global temperature (i.e., including all points on each model grid; Fig. 2a) show a dramatic negative shift in G1 experiment, indicating cooling at nearly all locations in the models compared with abrupt4×CO2. Under G4 the PDFs display discernible differences from rcp45, mainly as negative anomalies—but the change is much smaller in G4-rcp45 than in G1-abrupt4×CO2. The relationships remain the same over the ocean and land domains as in the global. Figures 2c and 2e reveal that differences between temperature extremes over ocean and land domains are small, but the PDFs are more strongly centrally peaked over land than over ocean.

The PDFs of monthly precipitation display smaller differences between the two experiments than for temperature (right-hand panels of Fig.2). The PDFs are positively skewed in all cases, a general characteristic of precipitation and other positive definite climate variables (e.g., wind speed). The largest difference between G1 and abrupt4×CO2 occurs over ocean, where low tails are shifted towards more negative precipitation anomalies in G1 (Fig. 2f). As in the case of temperature, changes under G4-rcp45 are much smaller than under G1-abrupt4×CO2 with only a slight negative shift. Fig. 2d & f show that there are almost no differences between G4 and rcp45 over both land and ocean.

3.3 Global mean time series

Figure 3 shows the differences (Δ) G1-abrupt4×CO2 and G4-rcp45 for TXx and TNn. In G1-abrupt4×CO2, ΔTNn is significantly negative (Fig. 3a), with a multimodel mean value of -5.1 ± 0.4 °C (one standard deviation, Table 3) over the 40 years analysis period (shaded region in Fig. 3a). By contrast, the extreme temperature index TXx has a smaller decrease with mean differences of -4.4 ± 0.3 °C. Multi-model mean values of ΔTNn are consistently a factor of ~1.2 more negative than those of ΔTXx (Fig. 3a and c), indicating a much stronger response of night-time low temperatures to a reduction in the solar constant, relative to daytime high temperatures. This is also the case in G4-rcp45, but with much smaller magnitude (ΔTNn = -0.7 ± 0.1 °C and ΔTXx = -0.6 ± 0.1 °C), Figs. 3b, d. The larger change in TNn relative to TXx was also found in the GeoMIP G1-piControl simulations analyzed by Curry et al. (2014), and in the increasing GHG scenarios in CMIP3 as well as CMIP5 (Tebaldi et al., 2006; Orlowsky and Seneviratne, 2012; Sillmann et al., 2013a). The explanation for the difference in daytime and night-time response is due to much stronger response of night-time low temperatures than daytime high temperatures. TNn is reduced more than TXx under G1 (and G4) because of the reduced warming under geoengineering, lower temperatures and reduced longwave effects throughout the whole day and night, although the reduced shortwave surface heating impacts daytime temperatures directly under G1 (and G4). The GISS-E2-R model has a noticeably weaker response measured by ΔTNn and ΔTXx changes than the other models. This is due to its relatively weak warming under abrupt4×CO2 as shown by Curry et al. (2014), meaning that the degree of solar dimming needed by G1 SRM is also weaker than for other models. The changes in radiative forcing at both short and long wavelengths are thus smaller in GISS-E2-R and the changes in various climate indicators are also smaller (Yu et al., 2015).

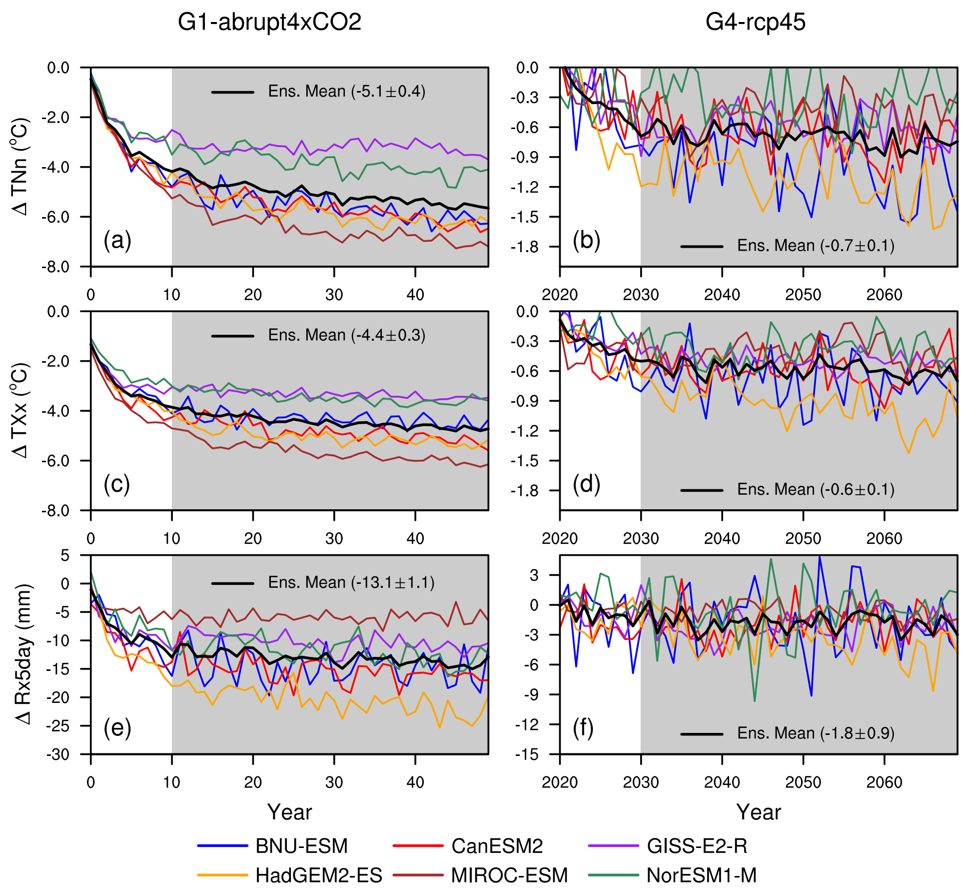

Figure 3: Time series of the difference of global mean extreme indices (as labelled on each left-hand panel's ordinate) between G1 - abrupt4×CO2 (left column) and G4 - rcp45 (right column) for all models analyzed. The black curves are the multimodel means, and gray shading indicates the 40-year analysis period for each experiment used in this study, with the ensemble mean value also shown on each panel.

The corresponding result for the extreme precipitation index, Rx5day is a significant reduction under G1 (Fig. 3e) with a multi-model mean value of -13.1±1.1 mm, indicating an overall weakening of the hydrological cycle. This feature was noted for non-extreme indices in the G1 experiments analyzed by

Schmidt et al. (2012) and Kravitz et al. (2013b). In contrast, the index for G4-rcp45 (Fig. 3f) is near-zero, though slightly negative on the whole, with the multi-model mean value of -1.8±0.9 mm. The partly positive Rx5day for G4-rcp45 reflects the climate variability simulated by models and lower signal-to-noise ratio. The mean temperature difference under G1 solar dimming is -4.3 °C, and -0.5 °C under G4 stratospheric aerosol, hence a ratio of 8.1, larger than extreme aspects of temperature: 7.3 for TNn, and 7.6 for TXx (Table 3). The corresponding ratio for mean precipitation is 7.0, whereas extreme precipitation indicated by Rx5day has a ratio of 7.3., similar to TNn and TXx. In general, G1 solar dimming and G4 stratospheric aerosol injection seem equally effective at changing extreme precipitation as well as extreme high and low temperatures, though solar dimming seems more effective than stratospheric aerosol injection at controlling mean temperature.

If relative humidity and atmospheric circulation remain relatively unchanged, then intense precipitation amount is governed by total precipitable water in the atmosphere, which the Clausius–Clapeyron relation says scales with mean temperatures (Allen and Ingram, 2002). The global mean precipitation decreases 2.1±0.4% per Kelvin in response to G1 solar dimming, and 2.7±1.0% per Kelvin in response to G4 stratospheric aerosol injection. The GISS-E2-R model contributes a relatively large portion to the spread of scaling between mean precipitation and temperature with a value of 4.5% per Kelvin for G4. If excluding the GISS-E2-R model, the global mean precipitation decreases 2.0±0.4% per Kelvin in response to G1 solar dimming, and 2.3±0.5% per Kelvin in response to G4 stratospheric aerosol injection. The scaling between mean precipitation and mean temperature under G1 and G4 is smaller than 3.4% precipitation change per Kelvin estimated from other coupled models under long-term equilibrium climate in response to doubling CO_2 (Allen and Ingram, 2002). The global mean Rx5day decreases 3.4±1.0% per Kelvin in response to G1 solar dimming, and 4.3±2.6% per Kelvin in response to G4 stratospheric aerosol injection. GISS-E2-R gives global mean Rx5day decreases 9.5% per Kelvin for G4. If excluding GISS-E2-R model, the global mean Rx5day decreases 3.4±1.1% per Kelvin in response to G1 solar dimming, and 3.3±0.6% per Kelvin in response to G4 stratospheric aerosol injection. The scaling of mean precipitation and mean temperature is expected to be much less than the 6.5% per Kelvin implied by the Clausius–Clapeyron relation, as the global-mean precipitation is primarily constrained by the availability of energy not moisture (Pall et al., 2007). The scaling of Rx5day and mean temperature under G1 and G4 is close to, but still weaker than the Clausius–Clapeyron relation, probably because Rx5day is not really an index of the heaviest rainfall events that are expected to be constrained by the

Clausius–Clapeyron relation. The Clausius–Clapeyron relation implies the same scaling of extreme precipitation and mean temperatures under both G1 and G4 experiments, which is the case here for five of six models, but not the GISS-E2-R model.

3.4 Spatial Response in Extremes

Geographical patterns of difference between the two SRM scenarios: i.e., G1- abrupt4×CO2 and G4-rcp45 are shown in Figure 4.

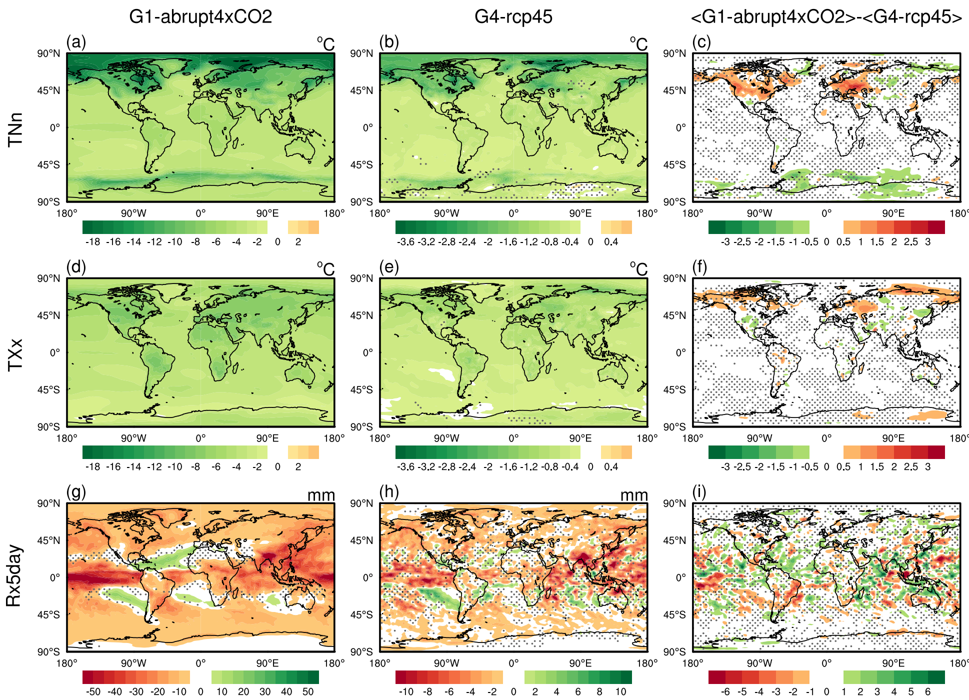

Figure 4: Geographical distributions over the 40-year analysis periods of the differences G1 - abrupt4×CO2 (left column), G4 - rcp45 (middle column), and differences between normalized G1 - abrupt4×CO2 and G4 - rcp45 (right column) for the extreme indices TNn (top row), TXx (middle row), and Rx5day (bottom row). Stippling indicates regions where fewer than 5 of 6 models agree on the sign of the model response. Note that panels have different colour scales.

The cooling patterns seen for TNn (Fig. 4a,b) are similar but with a larger signal for G1-abrupt4×CO2 than G4-rcp45, with the signature of polar amplification evident in both hemispheres but primarily in the Arctic. Several studies have considered the reasons behind this effect. Similar patterns occur in simulations of mean temperatures under both GHG warming scenarios and under geoengineering scenarios (Schmidt et al., 2012; Curry et al., 2014; Kravitz et al., 2013b). Pithan and Mauritsen (2014) conclude that in climate models it is primarily the temperature feedback with surface albedo of secondary importance in producing Arctic amplification under GHG forcing. While James et al. (2010) concluded that changes in sea ice cover play a leading role in recent Arctic temperature amplification for GHG forcing. The spatial pattern under geoengineering is due to the seasonal differences in longwave and shortwave forcing. Tilmes et al., (2014) and Hong et al., (2017) note the importance in poleward heat transport by reduction in the strength of the meridional overturning circulation under GHG forcing. Geoengineering has been shown to mitigate sea ice loss (Moore et al., 2014; Berdahl et al., 2014), and also reduce the decline in ocean poleward heat transport (Hong et al., 2017) relative to GHG forcing, but these changes do not completely counter the increase in radiative flux due to GHG forcing. In addition to the cooling patterns seen in the Arctic, TNn presents a cooling in the ocean around the Antarctica, which is not seen in TXx.

A notable feature in Fig. 4a, 4b, 4d and 4e is the larger cooling of TNn and TXx over land compared with oceans, also expressed in Table 3. The land-sea cooling contrast is larger for TXx than TNn (Fig 4d, e; Table 3), and TXx shows more uniform cooling than TNn across all latitudes. This feature is consistent with the stronger relationship of shortwave forcing to TXx. Under GHG warming scenarios, heat capacity differences, contrasts in surface sensible and latent fluxes, and boundary layer differences lead to contrasts opposite to those under G1 and G4 (Sutton et al., 2007; Joshi et al., 2008). Under G1 and G4, GHG warming occurs 24 hours a day, while reduced solar radiation is more effective in reducing day-time temperatures (TXx), with the land-sea heat capacity differences further enhancing TXx over TNx. The land–sea cooling effects under G4-rcp45 (Fig. 4b,4e) are consistent with Volodin et al. (2011) who found increased land–sea cooling contrast in annual mean temperature using the INMCM model forced with 4 Mt S/year equatorial stratospheric aerosol injection.

Comparing Figs. 4a,b and d,e shows that the magnitude of ΔTNn is larger than that of ΔTXx at high latitudes. The strongest cooling in TXx of up to -9.9°C under G1-abrupt4×CO2 (Fig. 4d) generally occurs in the interior of the continents as previously discussed, such as in South and North America, Eastern Europe, north-central Eurasia and Australia. The pattern is similar in G4-rcp45 but with a smaller magnitude. Fig. 4c, f show the differences between the normalized changes G1-abrupt4×CO2 and G4-rcp45. The stratospheric aerosol injection more effectively reduces the TNn in northern North America and western Europe compared with solar dimming, while the solar dimming more effectively reduces TNn in the Siberian coastal region, Eastern Antarctica and the adjacent ocean regions. The stratospheric aerosol also effectively reduces the TXx in northern North America and central Europe compared with solar dimming, but with a smaller spatial extent and magnitude compared with TNn. Stratospheric aerosol is more effective at reducing TXx in the Siberian coastal region, while the solar dimming seems more effective on reducing TNn there. Averaged over the globe, the magnitude of the extreme temperature anomalies under G1-abrupt4×CO2 is a factor of ~8 larger than under G4-rcp45, simply due to the much larger forcings in G1 relative to G4 (Table 3). Significantly smaller ratios for ΔTNn occur in central North America, eastern China and the northern Mediterranean as well as areas in Antarctica, with significantly larger ratios mainly in the Southern Ocean (not shown). Corresponding results for ΔTXx show smaller ratios in northern North America and Asia, West Asia, as well as areas in Antarctica, with larger ratios mainly in northeastern China and southern North America as well as in some ocean areas.

Using geoengineering to alleviate surface warming from increasing GHGs concentrations decreases global-mean precipitation (Schmidt et al., 2012; Kravitz et al., 2013b) as well as the wettest five days index (Rx5day), representing an extreme aspect of the precipitation distribution (Curry et al., 2014). The ensemble means show that Rx5day is strongly reduced over equatorial regions, especially in the equatorial Pacific and southern flank of the Tibetan Plateau (Fig. 4g,h). This is due to increased atmospheric stability and suppression of convection under geoengineering (Bala et al.,2008). Fig. 4g,h and Curry et al. (2014) show some robust increases in the tropics, northwest Africa, the Mediterranean Sea and areas of the subtropical oceans, which consistently display decreased Rx5day under abrupt4×CO2 compared to G1. This has been attributed to a weaker Hadley cell due to weaker radiative forcing (Tilmes et al., 2009), but more recent analysis of the tropical circulation suggests more complex interactions between radiative forcing and Hadley cell extent and intensity. Under GeoMIP G1 experiment, the Hadley cell edges remain at their preindustrial width latitudinally, despite the residual stratospheric cooling associated with elevated carbon dioxide levels (Davis et al., 2016; Guo et al., 2018). The damping of the seasonal migration of the Intertropical Convergence Zone (ITCZ) within the Hadley cell under G1 is associated with preferential cooling of the summer hemisphere (Smyth et al., 2017).

The spatial pattern for G4-rcp45 is not as coherent as that for G1-abrupt4×CO2, although Rx5day also increases mainly in the subtropics and decreases at equatorial regions, high latitudes and over most land areas (Fig. 4h). The noisy G4-rcp45 response is also seen in the climatological mean precipitation (Yu et al.,2014) under G3 and G4, as well as in the consecutive dry days (CDD) index under the G3 experiment (Aswathy et al., 2015). Furthermore, monsoonal regions including East Asia and India exhibit a reduction in Rx5day under G1-abrupt4×CO2, which may be attributed to a weakened monsoon. Tilmes et al. (2013)

observed, using a larger ensemble of models, that G1-abrupt4×CO2 results in a robust decrease in monsoonal precipitation, while it increases under abrupt4×CO2. Reduced Rx5day over monsoon regions is an indicator of weakened monsoon (Fig. 4g), because although the extreme precipitation index is calculated on an annual basis, it is dominated by wet season precipitation, particularly in monsoon areas (Klein Tank et al., 2006). However, the change under G4-rcp45 is not as robust (Fig. 4h), due at least partially to lower mean temperature changes and land-sea thermal contrast, and therefore smaller signal-to-noise ratios compared with G1-abrupt4×CO2. The difference between normalized change of G1-abrupt4×CO2 and G4-rcp45 is noisy and without coherent patterns (Fig. 4i).

As the tropical extreme precipitation change constitutes a large percentage of global extreme precipitation change in response to two type geoengineering schemes (Fig. 4g, 4h), it is interesting to know how the G1 solar dimming and G4 stratospheric aerosol injection affect major rain types in tropical regions. We compared tropical (± 30º lat.) relative frequency changes of four major daily rain types: light rain (<0.3 mm/day), moderate rain (0.9–2.4mm/day), heavy rain (>9mm/day) and an extremely heavy rain type (>24 mm/day) according to daily rain types used in Lau et al. (2013). All six models show consistent shift in rain regime, with a decrease in the frequency of extremely heavy rain by -22.3% for G1 and -3.6% for G4, heavy rain by -5.2% for G1 and -0.6% for G4, and consistent increase in the frequency of light rain by +4.4% for G1 and 0.5% for G4.

3.5 Extreme Duration Response

The TXx, TNn and Rx5day indices discussed above all characterize aspects of the absolute magnitude of climate extremes. We now analyze the duration indices shown in Figure 5: cold spell duration (CSDI), warm spell duration (WSDI), and consecutive dry days (CDD).

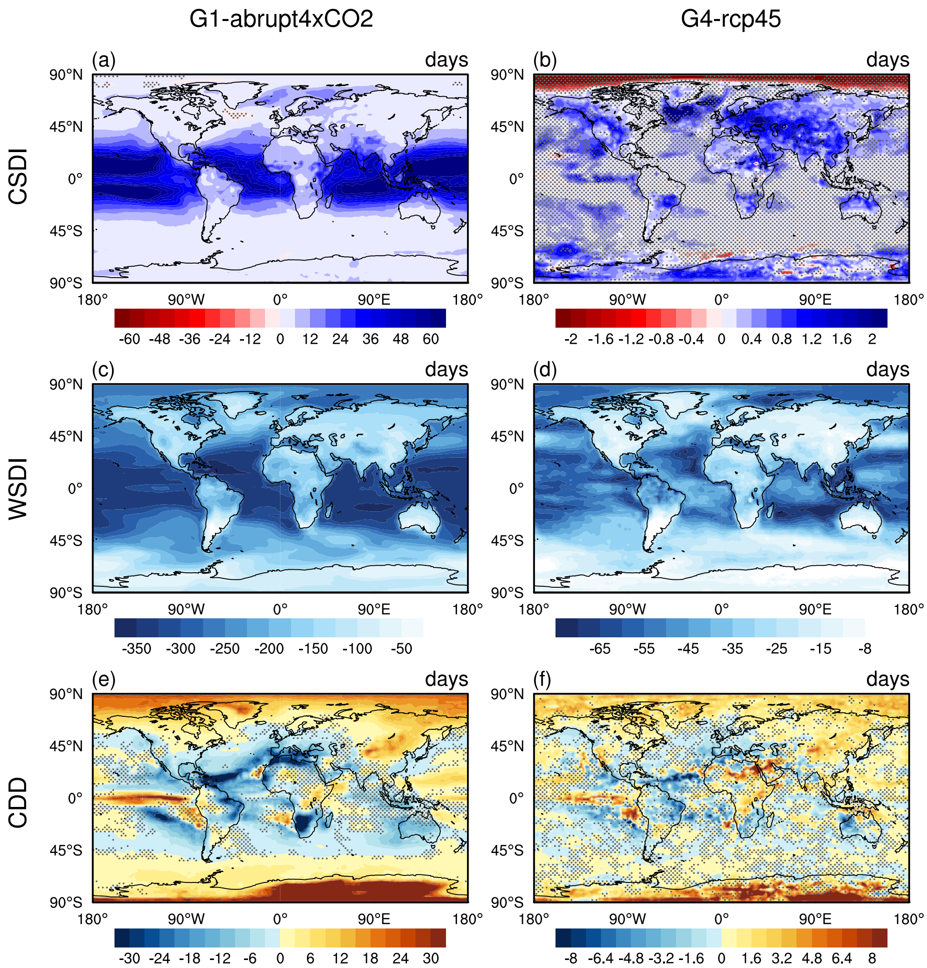

Figure 5: Geographical distributions of differences, G1 - abrupt4×CO2 (left column) and G4 - rcp45 (right column) for the extreme duration indices (a, b) CSDI, (c, d) WSDI, and (e, f) CDD, taken over the 40-year analysis periods. Stippling indicates regions where fewer than 5 of 6 models agree on the sign of the model response.

CSDI increases worldwide in the G1-abrupt4×CO2 anomaly (Fig. 5a), due to the strong negative shift of the PDF of surface temperature for G1 relative to abrupt4×CO2 (Fig. 1a). The most striking feature of Fig. 5a is the robust increase in CSDI over the tropical oceans with ΔCSDI exceeding 50 days per year over large regions, indicating that the region is sensitive to reduced solar radiation. Most of the CSDI differences over land in G1-abrupt4×CO2 are robust, with the notable exception of tropical regions such as India and Indonesia, which experience an increase in cold spell duration of more than 30 days (Fig. 5a). In contrast to the large response under G1-abrupt4×CO2, the pattern in G4-rcp45 is incoherent with wide disagreement about the sign of change between the models except for a robust increase over the continental regions of Eurasia and North America.

The spatial pattern of WSDI (Fig. 5c) shows a notable decrease over the tropical oceans, exceeding 300 days per year. The pattern is similar to CSDI but of larger magnitude and with a more widespread decrease over land areas such as eastern south America and the Tibetan Plateau (Fig. 5c). Comparison of Figs. 5a and 5c shows that in G1-abrupt4×CO2, WSDI decrease much more strongly over the tropical and subtropical oceans than do CSDI. The pattern of WSDI in G4-rcp45 is similar to that in G1-abrupt4×CO2, except in the equatorial ocean regions, which is also noticeable in the pattern of changes in CSDI (Figs. 5a, b).

The relatively small, but robust, changes in annual extreme temperature in the tropics apparently contradict the rather large robust increases in CSDI and decreases in WSDI (Fig. 5a, c) under solar dimming, but were also reported by Curry et al (2014). Cold spell and warm spell duration are related to the magnitude of changes in mean temperature relative to the short-term temperature variability. They are sensitive to the underlying climatological temperature variability of the respective region (Radinovio et al., 2012), which is small in the tropics and larger in the extra-tropics. A small shift in mean temperature can lead to large changes in the duration of cold and warm spells, which may have relatively large impacts on ecosystems (Corlett, 2011). The more robust results (lack of stippling in Fig. 5d) for the WSDI anomalies under G4 than for the CSDI are due to the significant cooling imparted by G4 relative to rcp45, as reflected by the color bar ranges. For example, BNU-ESM shows small increases in CSDI over the Arctic Ocean, while HadGEM2-ES shows strong decreases and other models have spatially varying results in G4 relative to rcp45. This may be due to Arctic amplification linked to, among other things discussed in Section 3.3, loss of sea ice, which occurs under both rcp45 and G4 simulations (Berdahl et al., 2014). There is a wide model spread in model-projected Arctic sea ice extent, although HadGEM2-ES and BNU-ESM produce similar sea ice patterns while MIROC-ESM simulates essentially no ice cover in autumn (Berdahl et al., 2014). The spatial pattern of the TOA net radiation flux varies relatively more in G4-rcp45, ranging from -0.22 to -0.56 Wm^{-2}, while comparatively ranging from -2.29 to -3.40 Wm^{-2} in G1-abrupt4×CO2 (Figure S1, S2 in Appendix). As simulation of sulphate aerosols differs among the participating G4 models, the spatially varying forcing results in very different cooling patterns particularly at high latitudes.

The equatorial Pacific in the vicinity of the ITCZ displays increases in CDD under G1-abrupt4×CO2 at the same locations (Fig. 5e) as Rx5day decreases (Fig. 4g). This may be related to the reduced latitudinal extent of seasonal movement of the ITCZ under G1 as noted in previous studies (Schmidt et al., 2012; Smyth et al., 2017). Anti-correlation between CDD and Rx5day can also be seen for decreases in CDD and increases in Rx5day in the tropical Atlantic, South Atlantic and the southeast Pacific dry zone. Both northern and southern high latitudes, and large parts of Eurasia display increases in CDD and decreases in Rx5day (Fig. 5e, 4g). CDD decreases in the desert regions of northern Africa, southwestern Africa, Australia and southwestern North America, which are strongly influenced by the descending branch of the tropical Hadley cell. This implies most places have fewer droughts under the geoengineering simulation than without it. Fig. 5f shows that the pattern in G4-rcp45 is similar to G1-abrupt4×CO2 but noisier.

3.6 Seasonality and zonal mean changes

We now examine the zonal structure and seasonality of changes in the climate extreme indices. Seasonal analysis is performed only for indices that can be presented on a monthly basis, i.e., TXx, TNn, and Rx5day. There are large temperature differences between G1 and abrupt4×CO2 simulations over polar regions due to residual polar amplification effects, and similarly for G4-rcp45 but with smaller magnitude.

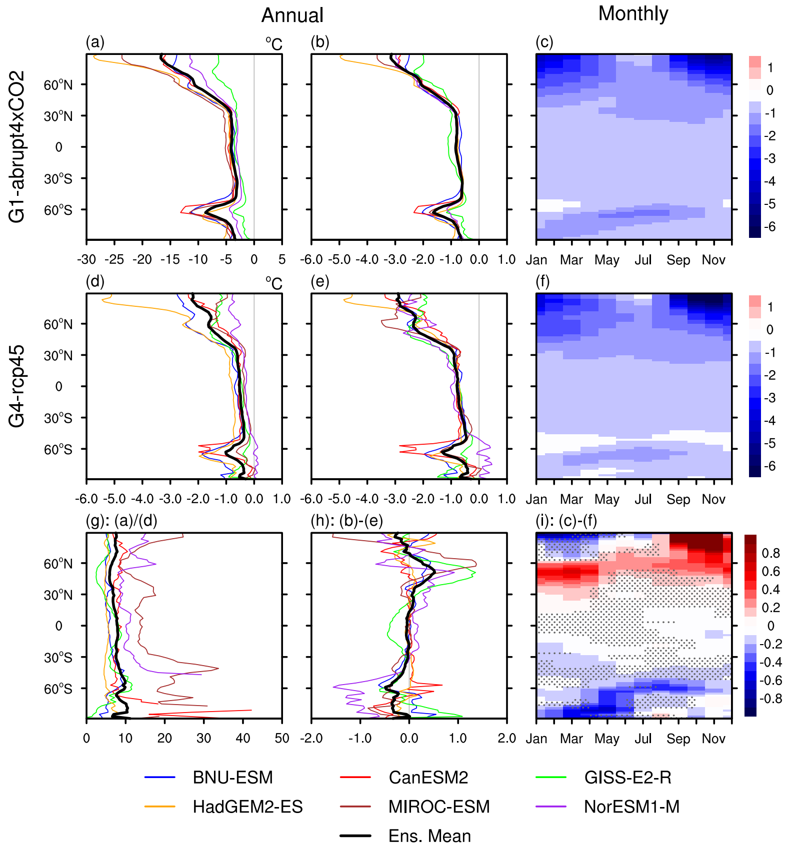

Figure 6: Absolute difference of annual zonal mean in the extreme low temperature TNn (left column), Normalized difference with respect to annual zonal mean (middle column) and monthly zonal mean (right column) in TNn: (a), (b), (c) G1 – abrupt4×CO2, (d), (e), (f) G4 – rcp45, (g) the ratio between absolute G1 – abrupt4×CO2 and G4 – rcp45, (h) the annual zonal mean difference between normalized G1 – abrupt4×CO2 and G4 – rcp45, (i) the monthly zonal mean difference between normalized G1 – abrupt4×CO2 and G4 – rcp45 taken over the 40-year analysis period. In panel (i) red colours indicate relatively greater changes with G4 and blue colours with G1, stippling indicates regions where fewer than 5 of 6 models agree on the sign of the model response. 3×3-point smoothing was applied to the seasonal-latitude change.

The left panels in Figure 6 display the zonal and annual mean anomalies, ΔTNn. The response in G1 compared with abrupt4×CO2 is of course uniformly negative (Fig. 6a), with multi-model mean annual peak values of -17°C near 90°N and -8°C near 65°S. In G4-rcp45, most models simulate a much smaller negative response.

As shown in the right panels of Fig. 6, the Arctic (defined as the region north of 67.5°N) cooling of TNn has a distinct seasonal character under both G1-abrupt4×CO2 and G4-rcp45. Arctic amplification peaks (up to -25°C in G1-abrupt4×CO2, and -5°C in G4-rcp45, not shown) in early winter (November to December). In winter under abrupt4×CO2, the warm ocean forms only limited seasonal sea ice cover and produces low cloud cover increasing downward longwave radiation and hence remains relatively warm. However, under G1 the sea ice cover is largely multi-year (Moore et al., 2014), hence is thicker and maintains a much lower surface temperature as the ice cover cools compared with open ocean. In summer, surface melting on the ice, which is still present in most models under abrupt4×CO2, and the large thermal inertia of the ocean tend to drive minimum surface temperatures under both G1 and abrupt4×CO2 close to the freezing point. A distinct TNn decrease is observed in the high latitudes of the Southern Ocean from April to October in both G1-abrupt4×CO2 and G4-rcp45, likely also due to sea ice processes. The annual zonal mean pattern of G4-rcp45 (Fig. 6d) is comparable to G1-abrupt4×CO2 (Fig. 6a), but weaker by a factor of 7 to 9 in terms of their absolute magnitudes (Fig. 6g). Fig. 6b, 6e show normalized zonal and annual mean anomalies of ΔTNn. Although G1 and G4 possess different geoengineering radiative forcings, the normalized zonal and annual mean anomalies of ΔTNn display similar patterns and magnitudes. The differences of normalized response in TNn in Fig. 6h is nearly spatially uniform, and close to zero in the annual mean, except for the high latitudes of the Northern and Southern Hemispheres. This is consistent with Fig. 6g, which shows the absolute ratio of response in TNn, and which implies that a constant scaling of the zonal and annual mean response to G4 would be close to that of G1. Hence, in Fig. 6i, values less than zero indicate where solar dimming is an intrinsically stronger geoengineering agent than stratospheric aerosols, and values above zero highlight where stratospheric aerosols tend to be more effective, with a value around zero meaning that solar dimming and stratospheric aerosols are equally effective. Fig. 6i shows that TNn in the northern high latitude springs and summers is affected much more by solar dimming than by stratospheric aerosol injection. A similar response is also present in the wintertime and springtime Southern Ocean. The only regions where stratospheric aerosol injection induces a significantly larger response than solar dimming is in the high Arctic in winter and latitudes between 40°-60°N in spring and winter, suggestive of a longwave radiative effect of the aerosols.

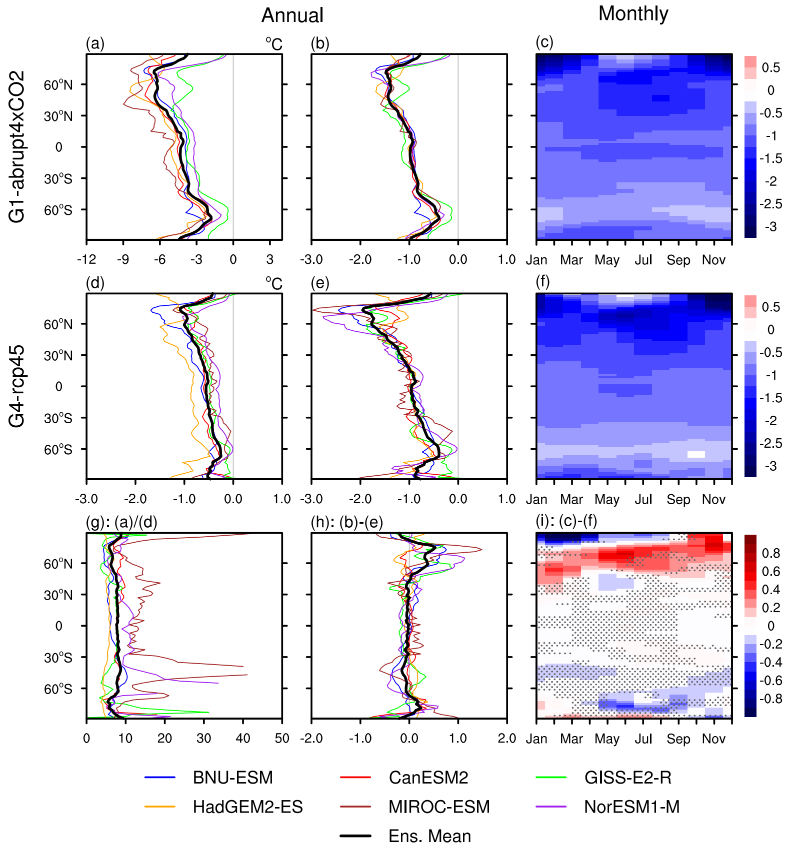

Figure 7: Absolute difference of annual zonal mean in the extreme high temperature TXx (left column), Normalized difference with respect to annual zonal mean (middle column) and monthly zonal mean (right column) in TXx: (a), (b), (c) G1 – abrupt4×CO2, (d), (e), (f) G4 – rcp45, (g) the ratio between absolute G1 – abrupt4×CO2 and G4 – rcp45, (h) the annual zonal mean difference between normalized G1 – abrupt4×CO2 and G4 – rcp45, (i) the monthly zonal mean difference between normalized G1 – abrupt4×CO2 and G4 – rcp45 taken over the 40-year analysis period. In panel (i) red colours indicate relatively greater changes with G4 and blue colours with G1, stippling indicates regions where fewer than 5 of 6 models agree on the sign of the model response. 3×3-point smoothing was applied to the seasonal-latitude change.

Figure 7 shows that the multi-model mean ΔTXx in both G1–abrupt4×CO2 and G4–rcp45 are of smaller magnitude than ΔTNn at high latitudes (Fig. 6). TXx is much less latitudinally variable than TNn both in G1-abrupt4×CO2 and G4-rcp45 (compare Figs. 6a, d and 7a, d). The signature of polar amplification (especially in the Northern Hemisphere) is evident in ΔTNn (Fig. 6a, d) whereas an asymmetric north – south response is evident for ΔTXx. The north-south ΔTXx asymmetry reflects the global land distribution, with ΔTXx more strongly affected over land than ocean (Fig. 4 d, e). The strongest cooling in G1-abrupt4×CO2 is found in Arctic winter, when more winter Atlantic cyclones track into the high Arctic under abrupt4×CO2 than G1 (Moore et al., 2014), and in the Northern mid-latitude summers, consistent with the regions where snow-albedo feedback and the soil moisture effect are strongest (Orlowsky and Seneviratne, 2012; Seneviratne et al., 2006; Diffenbaugh et al., 2007). Geoengineering leads to increases in both snow cover and soil moisture which lowers surface sensible heat flux, raises heat capacity and thus lowers sensitivity of temperature to radiative forcing changes (Curry et al., 2014, Dagon and Schrag, 2017). Similar patterns hold for G4-rcp45. As with TNn in Fig. 6h, the differences of normalized response in TXx is remarkably spatially uniform and around zero (Fig. 7h). Fig. 7i suggests that the relative effectiveness of stratospheric aerosols and solar dimming is similar, except for the Arctic, and perhaps Antarctica, where aerosols appear more effective than dimming in winter. Since the lack of shortwave radiative forcing during winter would not lead to differences in solar dimming or aerosol response, atmospheric circulation changes are implicated. The tropical lower stratospheric radiative heating due to stratospheric aerosol would drive a thermal wind response, which would intensify the stratospheric polar vortices. In contrast, solar dimming does not produce this effect and so there is little intensification of the polar vortex in G1. Therefore, the response of the northern hemisphere polar vortex to solar dimming geoengineering is much weaker than under stratospheric aerosol injection (Ferraro et al. 2015). A strengthening of the wintertime stratospheric polar vortices occurs under G4, tending to cool polar surface temperatures, which is consistent with wintertime northern hemisphere TNn and TXx patterns shown in Fig. 6i and 7i. This also promotes heterogeneous reactions on aerosols depleting stratospheric ozone, further strengthening the stratospheric vortex and cooling the poles (Tilmes et al., 2009), although this effect is not included in the models used in this study.

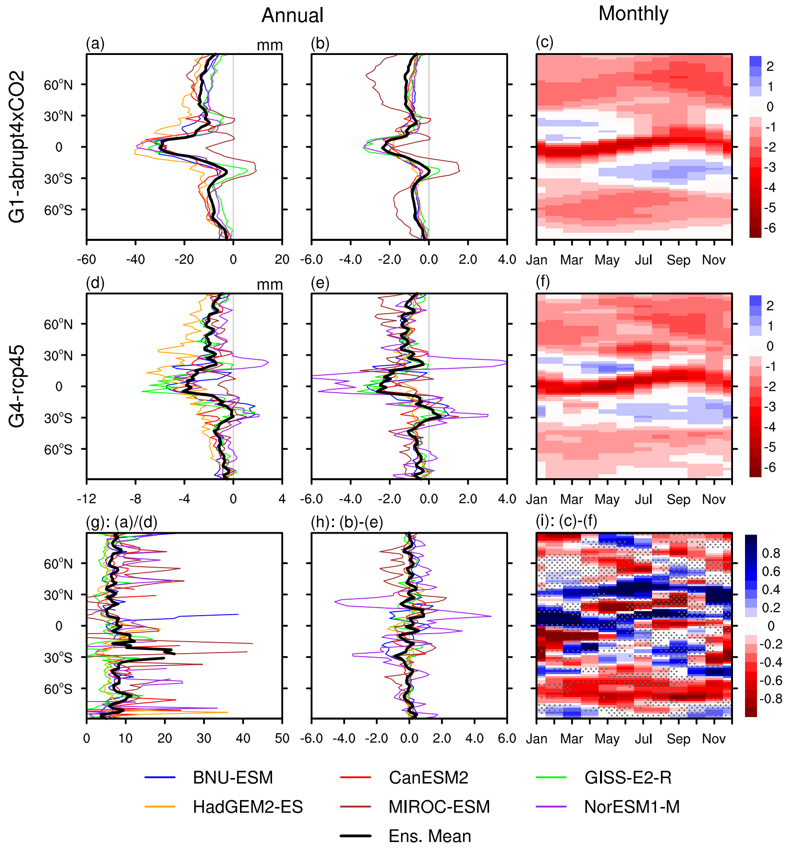

Figure 8: Absolute difference of annual zonal mean in the extreme precipitation Rx5day (left column), Normalized difference with respect to annual zonal mean (middle column) and monthly zonal mean (right column) in Rx5day: (a), (b), (c) G1 – abrupt4×CO2, (d), (e), (f) G4 – rcp45, (g) the ratio between absolute G1 – abrupt4×CO2 and G4 – rcp45, (h) the annual zonal mean difference between normalized G1 – abrupt4×CO2 and G4 – rcp45, (i) the monthly zonal mean difference between normalized G1 – abrupt4×CO2 and G4 – rcp45 taken over the 40-year analysis period. In panel (i) blue colours indicate relatively greater changes with G4 and red colours with G1, stippling indicates regions where fewer than 5 of 6 models agree on the sign of the model response. 3×3-point smoothing was applied to the seasonal-latitude change.

The results for the extreme precipitation index Rx5day are shown in Figure 8. Under GHG forcing alone, both observations and simulations show wet seasons get wetter and dry seasons get drier (Chou et al., 2013). The months July-November in the Northern Hemisphere and February-May in the Southern Hemisphere become somewhat drier (10-16%) under geoengineering. Fig. 8f displays a similar summer/winter, tropical wet/dry season effect for G4, where it appears over a slightly narrow latitude range and is slightly delayed relative to G1. Increased occurrence of extreme rainfall under G1 (>16%) is expected during winter and spring for the subtropical regions of both hemispheres. The effect on Rx5day is largest in April to November in the Southern Hemisphere, which roughly corresponds with the subtropical wet season. The path of darker red in Figs 8c and 8f appear to follow quite closely the seasonal migration of the ITCZ which wanders near the sub-solar point. Smyth et al. (2017) report that the seasonal amplitude of migration of the ITCZ is reduced under G1 relative to piControl and this would be consistent with the seasonal reduction in Rx5day along the dark red paths in Figs 8c and 8f. Tilmes et al. (2013) noted that in the G1 experiment precipitation in the tropics is reduced by around 5% with a larger interannual variability and spread among the models over land compared to the ocean. Furthermore there is considerable reduction in frequency of heavy precipitation (> 8 mm day^{-1}) over the tropics and at the same time an increase in the frequency of small and moderate precipitation intensity. This is consistent with the seasonal analysis shown in Fig. 8 if the extreme precipitation events are generally occurring in the wet season, while the small and moderate events primarily occur in the dry seasons.

Prominent decreases in Rx5day are observed year-round at high latitudes consistent with general drying under both geoengineering scenarios. Fig. 8g, 8h shows that the zonal means are noisier than for TNn and TXx. The results look much more complex than the temperature extreme indices in Fig. 6h and 7h. The general effect is that the tropical regions (30ºS-30ºN) are more strongly affected by aerosol injection than by solar dimming. The mid-latitude Rx5day is more effectively changed by stratospheric aerosol injection geoengineering year-round, especially in the Northern Hemisphere. Except for summertime polar areas, solar dimming geoengineering is relatively more effective year-round at high-latitudes, especially in the Southern Hemisphere. Ferraro et al. (2014) found that the tropical overturning circulation weakens in response to geoengineering with stratospheric sulphate aerosol injection due to radiative heating from the aerosol layer, but geoengineering simulated as a simple reduction in total solar irradiance do not capture this effect. Therefore, a relatively large tropical precipitation perturbation occurs under stratospheric aerosol injection. On the other hand, the meridional distribution of the sulphate aerosols is handled different between the models (as outlined in Section 3.1), which also contributes the noisier Rx5Day pattern showing in Fig. 8d, 8g and 8i. Four of the six models (BNU-ESM, CanESM2, MIROC-ESM and NorESM1-M) analysed in our study use the AOD prescribed to mimic the one-fourth of the 1991 eruption of Mount Pinatubo, but with different AOD meridional distribution, particle effective radii, and standard deviations of their log-normal size distribution (Kashimura et al., 2017). Another two models (GISS-E2-R and HadGEM2-ES) adopt different stratospheric aerosol schemes to simulate the sulphate AOD.

Stratospheric sulphate aerosols result in heating of the stratosphere, particularly in the tropics, (e.g., Tilmes et al., 2009). Changes in heating rates in the stratosphere and at the tropopause would directly change the tropospheric lapse rate, likely altering the stability of the atmosphere, relative humidity and hence the hydrological cycle. The Northern Hemisphere peak tropical cyclone (TC) season is August through October, and the Southern Hemisphere season is January through March. Interestingly, the Southern Hemisphere ocean basins (5-20°S) where TCs are generated are red in Fig. 8i during the TC season, while in the Northern Hemisphere the TC basins are blue in their TC season. This suggests a dichotomy between the hemispheres insofar as the type of geoengineering that may moderate tropical storms and hurricanes: these are more effectively moderated in the Northern Hemisphere by G4 stratospheric aerosol injection and in the Southern Hemisphere by G1 solar dimming. We have no mechanism for this response, but we note that the response of TC varies between basins with notable hemispheric differences in response to G4 and rcp45 (Wang et al., 2018).

Analysis of the 1991 Pinatubo and 1982 El Chichón volcanic eruptions by Evan (2012) revealed significant reduction in TC number ($p<0.01$) in Atlantic hurricane frequency duration and intensity in the three following seasons compared with the three prior to the eruptions. This corresponds with reduced cyclogenesis in the region 8°-20°N during July-November, driven by decreases in sea surface temperatures of about 0.8°C and stratospheric warming (at 70 hPa) of about 3°C caused by the volcanic aerosol direct effect. The G4 experiment is equivalent to about one-quarter of the 1991 Pinatubo eruption, so the effects would be much weaker, consistent with the modest changes seen in Fig. 8f. The greater effectiveness of G4 stratospheric aerosol than G1 solar dimming in changing Rx5day (Fig. 8i) during July-November in the northern tropics is suggestive that both the sea surface temperature reduction and the stratospheric heating are playing significant roles in changing tropical cyclogenesis.

In summary, the normalized zonal mean annual responses in TNn, TXx and to a lesser extent for Rx5day show similar meridional structure and magnitude for solar dimming and stratospheric aerosol injection geoengineering (Fig. 6h, 7h, 8h), with the exception of Northern Hemisphere high latitudes where the two geoengineering methods show different effectiveness in moderating the seasonality of TNn and TXx.

4 Summary and conclusions

We have compared the impacts of reduced solar radiation (G1) and stratospheric aerosol injection (G4) on temperature and precipitation extremes in corresponding reference experiments (abrupt4×CO2 and rcp45, respectively), particularly their spatial and temporal patterns. Most previous studies comparing solar dimming and stratospheric aerosol SRM have concentrated on the climate mean response (Jones et al., 2011; Niemeier et al., 2013; Ferraro et al., 2014). Curry et al. (2014) examined the effect of G1 geoengineering on the same metrics of extreme temperature and precipitation response (both magnitude and duration) as examined here, but did not compare the responses of solar dimming and stratospheric aerosol injection that we focus on in this paper.

Despite large difference in the magnitude of the response induced by the two geoengineering schemes (which is somewhat larger than the ratio of the input forcings), our results show that the patterns of extreme high and low temperature in solar dimming and stratospheric aerosol injection geoengineering schemes are geographically similar, with regional differences mostly over high latitudes. Solar dimming SRM is relatively more effective in reducing night-time temperatures (TNn) in high-latitude summer, especially in the Arctic. There are much smaller differences in the effectiveness of aerosol and dimming SRM for the warmest day (TXx), though high latitude winters are more affected by stratospheric aerosols than solar dimming.

As reflected by the wettest consecutive five days index Rx5day, both SRM methods have a moderating effect on extreme precipitation during the hurricane/typhoon seasons for both hemispheres. Stratospheric aerosol injection is more effective at reducing precipitation during the Northern Hemisphere TC season, while months outside the hurricane season are wetter under solar dimming, and vice versa in the Southern Hemisphere. Despite their different responses, both G1 and G4 moderate Rx5day in the cyclone season while increasing it other months, thus both schemes affect tropical cyclogenesis. Relative differences under both SRM methods are larger in precipitation extremes than for temperature extremes. This may be because, in addition to the cooling of sea surface temperatures facilitated by both solar dimming and stratospheric aerosol injection, stratospheric aerosol injection heats the stratosphere via absorbing near infrared and longer wavelengths radiation (Lohmann and Feichter, 2005). This mechanism is present in all models analyzed here. This finding suggests that models that rely only on parameterizing hurricane numbers and intensity by surface temperatures (Moore et al., 2015) are likely to underestimate the impact of stratospheric aerosol geoengineering compared with comparable amounts of solar dimming, though there are very large differences in how both greenhouse gas warming and stratospheric aerosol injection affects cyclogenesis across the different tropical basins (Wang et al., 2018).

Davis et al (2016) and Smyth (2017) examined the changes in the mean state of the tropical Hadley cells to GHG forcing and the G1 scenario. They note that the poleward expansion of the Hadley cell occurs under the GHG forcing, but under G1 it is indistinguishable from the preindustrial control state, and moreover find that the ITCZ is reduced in its seasonal migration amplitude under G1 but not GHG forcing. Further analysis of the Hadley and Walker cell intensities under G1 (Guo et al., 2018) shows that the Hadley circulation is reduced under G1 relative to piControl, but that changes under GHG forcing are rather more complex, affecting also the higher latitude Ferrel cells. Thus, some of the relative differences seen in the extreme indices around the tropics may reflect a tendency of geoengineering to mitigate changes in the Hadley cell caused by GHG forcing.

The hydrological cycle strength weakens under both types geoengineering. In our analysis, the global mean precipitation decrease per Kelvin is stronger in response to G4 stratospheric aerosol than to G1 solar dimming. This is consistent with a previous study by Niemeier et al. (2013), in which impacts on energy balance and hydrological cycle by three different solar geoengineering schemes are examined. The differences between stratospheric aerosol injection and solar dimming are influenced strongly by the absorption of longwave radiation by aerosols, this atmospheric heating imbalance could further stabilize the troposphere and lead to stronger precipitation reduction under stratospheric aerosol injection than under solar dimming (Niemeier et al., 2013). Recently Xia et al. (2018) found precipitation and evaporation changes are very similar under sulphate and solar dimming geoengineering schemes using the full tropospheric and stratospheric chemistry version of the Community Earth System Model (CESM). This is different from previous studies by Niemeier et al. (2013) and Ferraro et al. (2014), who found that the sulphate geoengineering has larger effect on the hydrological cycle. Xia et al. (2018) suggested that the column ozone change could possibly play an important role in a fully coupled atmosphere–chemistry model by changing radiative forcing and atmospheric lapse rate, while in Niemeier et al. (2013) and Ferraro et al. (2014) the same prescribed ozone was used in all scenarios. In our study, according to the scaling of global mean precipitation reduction to mean temperature change, all models show a relatively larger reduction of global mean precipitation per Kelvin under stratospheric aerosol injection than under solar dimming, which is consistent with Niemeier et al. (2013) and Ferraro et al. (2014). Among six GeoMIP models used here, only GISS-E2-R model calculates ozone for its G4 simulation, other models and experiments all use prescribed ozone. Therefore, we cannot diagnose ozone's roles as suggested by Xia et al. (2018).

Compared with solar dimming SRM, aerosol SRM has larger differences between models and a much lower signal-to-noise ratio, although the aerosol geoengineering applied was of a much smaller magnitude than the solar dimming. Aerosol SRM was relatively less effective in increasing cold spell duration and decreasing warm spell duration in equatorial oceans than solar dimming, consistent with a relatively smaller cooling effect in coldest day and warmest night in equatorial oceans than in adjacent regions. The reduced cooling effect in equatorial oceans in aerosol SRM may result from the smaller reduction in shortwave radiation flux at the top of atmosphere in aerosol SRM in these regions.

Climate extremes are more readily perceived by society and can have more immediate economic and social impacts than changes in mean climate (IPCC, 2012). Yet, the ETCCDI extreme climate indices may not reflect what are considered "extreme events" by the public. These would include events such as typhoons, severe heatwaves etc., that may occur much less frequently, but are of higher intensity, than the thresholds represented by the indices used here. The downscaling and impact modelling required to assess geoengineered climate effects has so far been limited to a study of Atlantic hurricane storm surge size and frequency (Moore et al., 2015), but such studies are a clear focus of ongoing research. More climate models with various aerosol parameterization schemes are certainly needed to describe the extreme tails of simulated climate variables. These extremes are incompletely sampled from 40-year long periods of model runs, but may be explored more thoroughly by specific impact models driven by the thermodynamic state of the climate system (Emanuel, 2013), and by planned extensions to the G1 experiment outlined under GeoMIP6 (Kravitz et al., 2015).

Acknowledgements

We thank all participants of the Geoengineering Model Intercomparison Project and their model development teams, the CLIVAR/WCRP Working Group on Coupled Modelling for endorsing GeoMIP, and the scientists managing the Earth System Grid data nodes who have assisted with making GeoMIP output available. Research was funded by the National Basic Research Program of China grant number 2015CB953600. HK and SW were supported by the SOUSEI Program, MEXT, Japan. CC is supported by the NSERC-funded Canadian Sea Ice and Snow Evolution Network. HM was supported by Research Council of Norway grant 229760/E10, and Sigma2 HPC resources hexagon and norstore (accounts nn9812k, nn9448k, NS9033K). MIROC-ESM simulations were conducted using the Earth Simulator. We thank Andy Jones for model development and comments on the manuscript. The Pacific Northwest National Laboratory is operated for the U.S. Department of Energy by Battelle Memorial Institute under contract DE-AC05-76RL01830.

Appendix: TOA net radiation flux differences of G1-abrupt4×CO2 and G4-rcp45 for each model

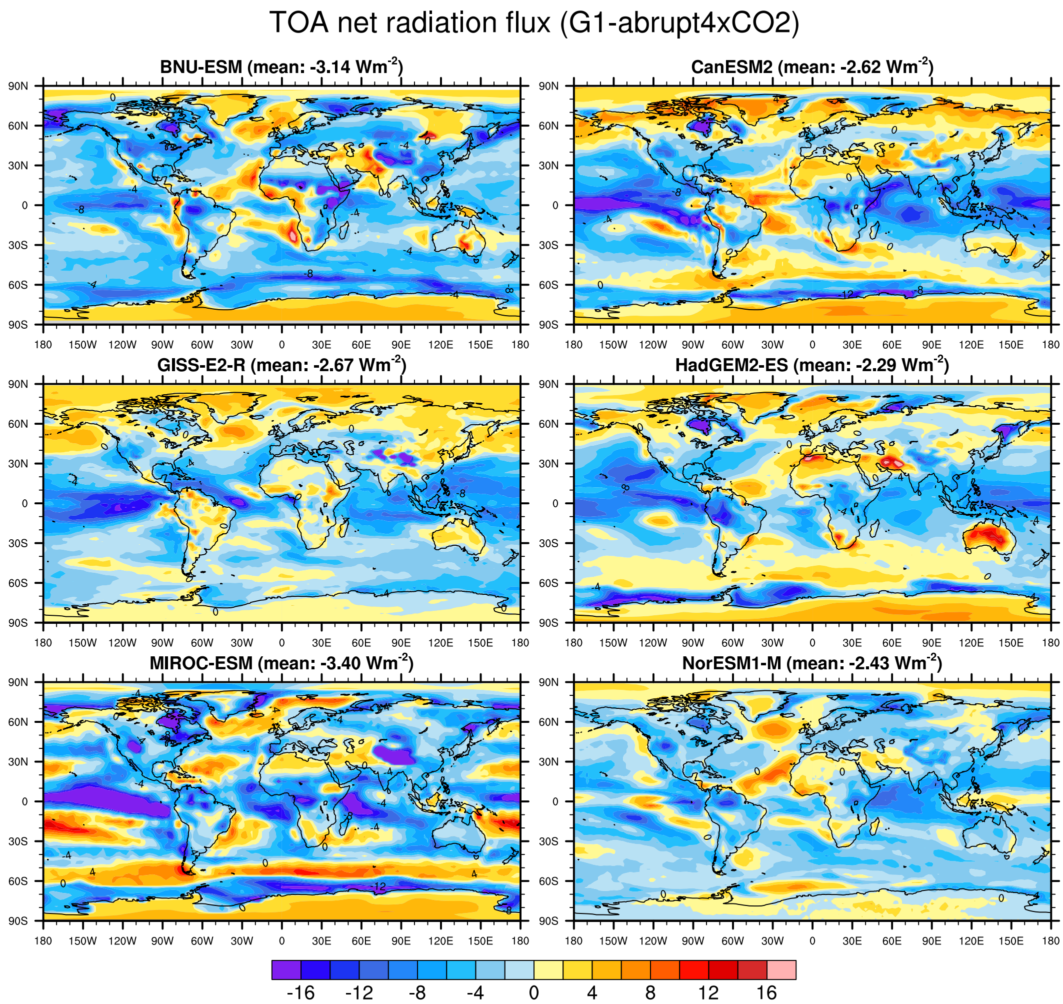

Figure S1: Geographical distributions over the 40-year analysis periods of the differences G1 - abrupt4×CO2 for TOA net radiation flux for BNU-ESM, CanESM2, GISS-E2-R, HadGEM2-ES, MIROC-ESM and NorESM1-M.

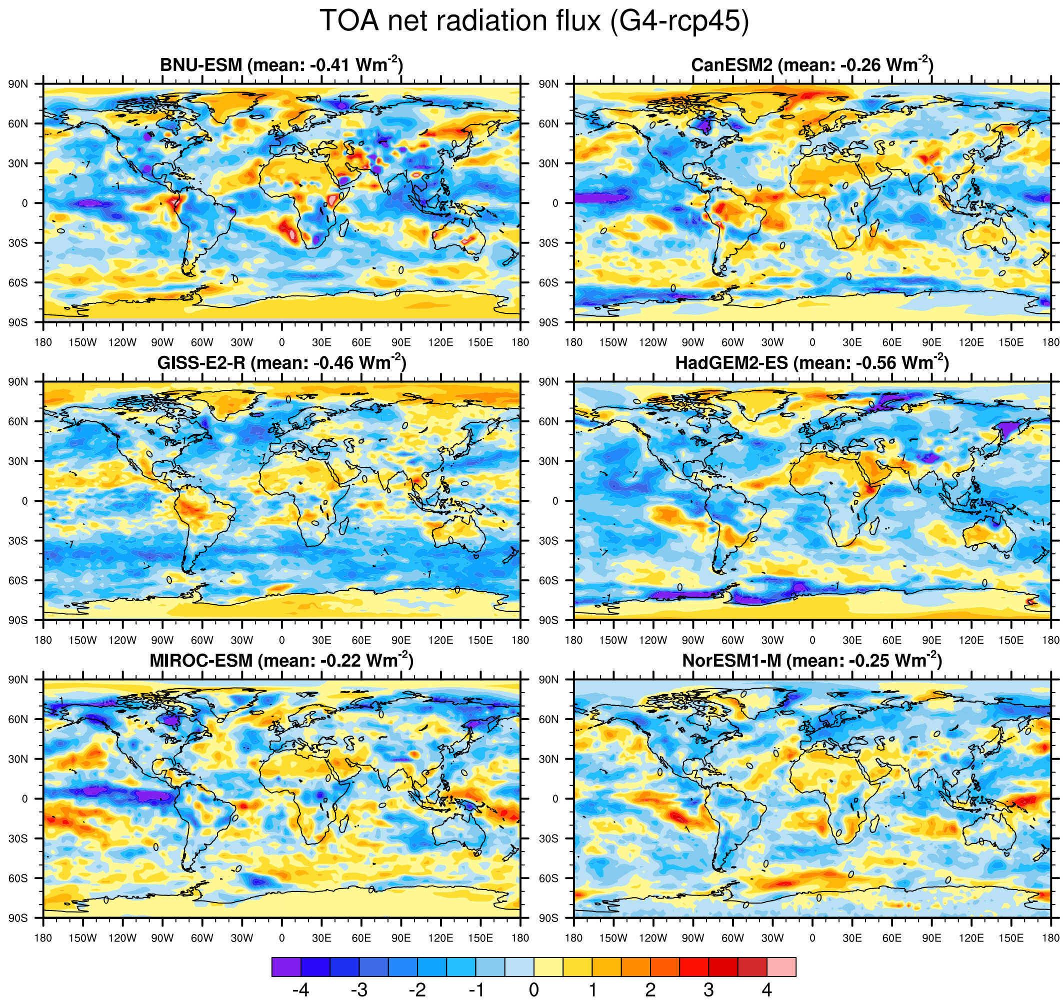

Figure S2: Geographical distributions over the 40-year analysis periods of the differences G4 – rcp45 for TOA net radiation flux for BNU-ESM, CanESM2, GISS-E2-R, HadGEM2-ES, MIROC-ESM and NorESM1-M.

References

Allen, M. and Ingram, W.: Constraints on future changes in climate and the hydrologic cycle, Nature, 419, 224–232, 2002.

Arora, V. K., Scinocca, J. F., Boer, G. J., Christian, J. R., Denman, K. L., Flato, G. M., Kharin, V. V., Lee, W. G., and Merryfield, W. J.: Carbon emission limits required to satisfy future representative concentration pathways of greenhouse gases, Geophys. Res. Lett., 38, L05805, 2011.

Aswathy, V. N., Boucher, O., Quaas, M., Niemeier, U., Muri, H., Mülmenstädt, J., and Quaas, J.: Climate extremes in multi-model simulations of stratospheric aerosol and marine cloud brightening climate engineering, Atmos. Chem. Phys., 15, 9593–9610, doi:10.5194/acp-15-9593-2015, 2015.

Bala, G., Duffy, P. B., and Taylor, K. E.: Impact of geoengineering schemes on the global hydrological cycle, Proc. Natl. Acad. Sci., 105,7664–7669, doi:10.1073/pnas.0711648105, 2008.

Berdahl, M., Robock, A., Ji, D., Moore, J., Jones, A., Kravitz, B., and Watanabe, S.: Arctic cryosphere response in the Geoengineering Model Intercomparison Project (GeoMIP) G3 and G4 scenarios, J. Geophys. Res. –Atmos., 119, 1308-1321, doi: 10.1002/2013JD020627, 2014.

Bentsen, M., Bethke, I., Debernard, J. B., Iversen, T., Kirkevåg, A., Seland, Ø., Drange, H., Roelandt, C., Seierstad, I. A., Hoose, C., and Kristjánsson, J. E.: The Norwegian Earth System Model, NorESM1-M – Part 1: Description and basic evaluation of the physical climate, Geosci. Model Dev., 6, 687-720, https://doi.org/10.5194/gmd-6-687-2013, 2013.

Budyko, M. I.: Climatic Changes, American Geophysical Union, Washington D.C. 1977.

Collins, W. J., Bellouin, N., Doutriaux-Boucher, M., Gedney, N., Halloran, P., Hinton, T., Hughes, J., Jones, C. D., Joshi, M., Liddicoat, S., Martin, G., O'Connor, F., Rae, J., Senior, C., Sitch, S., Totterdell, I., Wiltshire, A., and Woodward, S.: Development and evaluation of an Earth-System model – HadGEM2, Geosci. Model Dev., 4, 1051-1075, doi:10.5194/gmd-4-1051-2011, 2011.

Corlett, R. T.: Impacts of warming on tropical lowland rainforests, Trends Ecol. Evol., 26, 606–613, doi:10.1016/j.tree.2011.06.015, 2011.

Crutzen, P. J.: Albedo enhancement by stratospheric sulfur injections: a contribution to resolve a policy dilemma? Clim. Chang., 77, 211–219, doi:10.1007/s10584-006-9101-y, 2006.

Curry, C. L., Sillmann, J., Bronaugh, D., Alterskjaer, K., Cole, J.N. S., Ji, D., Kravitz, B., Kristjánsson, J. E., Moore, J. C., Muri, H., Niemeier, U., Robock, A., Tilmes, S., and Yang, S.: A multimodel examination of climate extremes in an idealized geoengineering experiment, J. Geophys. Res. -Atmos., 3900–3923, doi:10.1002/2013JD020648, 2014.

Davis, N. A., Seidel, D. J., Birner, T., Davis, S. M., and Tilmes, S.: Changes in the width of the tropical belt due to simple radiative forcing changes in the GeoMIP simulations, Atmos. Chem. Phys., 16, 10083-10095, doi:10.5194/acp-16-10083-2016, 2016.

Dagon, K., and Schrag, D. P.: Regional climate variability under model simulations of solar geoengineering, J. Geophys. Res. –Atmos., 122, doi:10.1002/2017JD027110, 2017.

Diffenbaugh, N. S., Pal, J. S., Giorgi, F., and Gao, X. J.: Heat stress intensification in the Mediterranean climate change hotspot, Geophys. Res. Lett., 34, L11706, doi:10.1029/2007GL030000, 2007.

Donat, M. G., Alexander, L. V., Yang, H., Durre, I., R. Vose, and Caesar, J.: Global land-based datasets for monitoring climatic extremes, Bull. Am. Meteor. Soc., 94, 997-1006, doi:10.1175/BAMS-D-12-00109.1, 2013.

Emanuel, K. A.: Downscaling CMIP5 climate models shows increased tropical cyclone activity over the 21st century, PNAS, 110, 12219-12224, doi:10.1073/pnas.1301293110, 2013.

Evan, A. T.: Atlantic hurricane activity following two major volcanic eruptions, J. Geophys. Res., 117, D06101, doi:10.1029/2011JD016716, 2012.

Ferraro, A. J., Highwood, E. J., and Charlton-Perez, A. J.: Weakened tropical circulation and reduced precipitation in response to geoengineering, Environ. Res. Lett., 9, doi:10.1088/1748-9326/9/1/014001, 2014.

Ferraro, A. J., Charlton-Perez, A. J. and Highwood, E. J.: Stratospheric dynamics and midlatitude jets under geoengineering with space mirrors and sulfate and titania aerosols, J. Geophys. Res. Atmos., 120, 414–429, doi:10.1002/2014JD022734, 2015.

Frich, P., Alexander, L. V., Della-Marta, P., Gleason, B., Haylock, M., Tank, A., and Peterson, T.: Observed coherent changes in climatic extremes during the second half of the twentieth century, Clim. Res., 19, 193–212, doi:10.3354/cr019193, 2002.

Guo, A., Moore, J. C., Ji, D.: Tropical atmospheric circulation response to the G1 sunshade geoengineering radiative forcing experiment, Atmos. Chem. Phys., doi:10.5194/acp-2018-141, 2018.

Hong, Y., Moore, J. C., Jevrejeva, S., Ji, D., Phipps, S. J., Lenton, A., Tilmes, S., Watanabe, S. and Zhao, L.: Impact of the GeoMIP G1 sunshade geoengineering experiment on the Atlantic meridional overturning circulation, Environ. Res. Lett. 12, 034009, doi: 10.1088/1748-9326/aa5fb8, 2017.

IPCC, Managing the Risks of Extreme Events and Disasters to Advance Climate Change Adaptation, A Special Report of Working Groups I and II of the Intergovern mental Panel on Climate Change, Cambridge Univ. Press, Cambridge and New York ,2012.

Irvine, P. J., Ridgwell, A., and Lunt, D. J.: Assessing the regional disparities in geoengineering impacts, Geophys. Res. Lett., 37, 1–6, doi:10.1029/2010GL044447, 2010.

James, A. S. and Simmonds, I.: The central role of diminishing sea ice in recent Arctic temperature amplification, Nature, 464, 1334–1337, doi:10.1038/nature09051, 2010.

Ji, D., Wang, L., Feng, J., Wu, Q., Cheng, H., Zhang, Q., Yang, J., Dong, W., Dai, Y., Gong, D., Zhang, R.-H., Wang, X., Liu, J., Moore, J. C., Chen, D., and Zhou, M.: Description and basic evaluation of

Beijing Normal University Earth System Model (BNU-ESM) version 1, Geosci. Model Dev., 7, 2039-2064, doi:10.5194/gmd-7-2039-2014, 2014.

Jones, A., Haywood, J., and Boucher, O.: A comparison of the climate impacts of geoengineering by stratospheric SO_2 injection and by brightening of marine stratocumulus cloud, Atmos. Sci. Lett., 12, 176–183, doi:10.1002/asl.29, 2011.

Jones, A., Haywood, J. M., Alterskjaer, K., Boucher, O., Cole, J. N. S., Curry, C. L., Irvine, P. J., Ji, D., Kravitz, B., Egill Kristjánsson, J., Moore, J. C., Niemeier, U., Robock, A., Schmidt, H., Singh, B., Tilmes, S., Watanabe, S., and Yoon, J.-H.: The impact of abrupt suspension of solar radiation management (termination effect) in experiment G2 of the Geoengineering Model Intercomparison Project (GeoMIP), J. Geophys. Res. -Atmos., 118, 9743– 9752, doi:10.1002/jgrd.50762, 2013.

Jones, P. W.: First- and second-order conservative remapping schemes for grids inspherical coordinates, Mon. Weather Rev., 127, 2204–2210, doi:10.1175/1520-0493, 1999.

Joshi, M. M., Gregory, J. M., Webb, M. J., Sexton, D. M. H., and Johns, T. C.: Mechanisms for the land/sea warming contrast exhibited by simulations of climate change, Clim. Dyn., 30, 455–465, doi:10.1007/s00382-007-0306-1, 2008.

Kashimura, H., Abe, M., Watanabe, S., Sekiya, T., Ji, D., Moore, J. C., Cole, J. N. S., and Kravitz, B.: Shortwave radiative forcing, rapid adjustment, and feedback to the surface by sulfate geoengineering: analysis of the Geoengineering Model Intercomparison Project G4 scenario, Atmos. Chem. Phys., 17, 3339–3356, doi:10.5194/acp-17-3339-2017, 2017.

Klein Tank, A. M. G., Peterson, T. C., Quadir, D. A., Dorji, S., Zou, X., Tang, H., Santhosh, K., Joshi, U. R., Jaswal, A. K., Kolli, R. K., Sikder, A. B., Deshpande, N. R., Revadekar, J. V., Yeleuova, K., Vandasheva, S., Faleyeva, M., Gomboluudev, P., Budhathoki, K. P., Hussain, A., Afzaal, M., Chandrapala, L., Anvar, H., Amanmurad, D., Asanova, V. S., Jones, P. D., New, M. G., and Spektorman, T.: Changes in daily temperature and precipitation extremes in central and south Asia, J. Geophys. Res., 111, D16105, doi:10.1029/2005JD006316, 2006.

Kravitz, B., Robock, A., Boucher, O., Schmidt, H., Taylor, K. E., G. Stenchikov, and Schulz, M.: The Geoengineering Model Intercomparison Project (GeoMIP), Atmos. Sci. Let., doi:10.1002/asl.316, 2011.

Kravitz, B., Robock, A., Forster, P. M., Haywood, J. M., Lawrence, M. G., and Schmidt, H.: An overview of the Geoengineering Model Intercomparison Project (GeoMIP), J. Geophys. Res. -Atmos., 118, 13103–13107, doi:10.1002/2013JD020569, 2013a.

Kravitz, B., Caldeira, K., Boucher, O., Robock, A., Rasch, P. J., Alterskjær, K., Karam, D. B., Cole, J. N. S., Curry, C. L., Haywood, J. M., Irvine, P. J., Ji, D., Jones, A., Kristjánsson, J. E., Lunt, D. J., Moore, J. C., Niemeier, U., Schmidt, H., Schulz, M., Singh, B. Tilmes, S., Watanabe, S., Yang, S., and Yoon, J.: Climate model response from the geoengineering model intercomparison project (GeoMIP), J. Geophys. Res. -Atmos., 118, 8320-8332. doi:10.1002/jgrd.50646, 2013b.

Kravitz, B., Forster, P. M., Jones, A., Robock, A., Alterskjær, K., Boucher, O., Jenkins, A. K. L., Korhonen, H., Kristjánsson, J. E., Muri, H., Niemeier, U., Partanen, A., Rasch, P. J., Wang, H., and Watanabe, S.: Sea spray geoengineering experiments in the geoengineering model intercomparison project (GeoMIP): Experimental design and preliminary results, J. Geophys. Res. -Atmos., 118, 11175–11186, doi:10.1002/jgrd.50856, 2013c.

Kravitz, B., Robock, A., Tilmes, S., Boucher, O., English, J. M., Irvine, P. J., Jones, A., Lawrence, M. G., MacCracken, M., Muri, H., Moore, J. C., Niemeier, U., Phipps, S. J., Sillmann, J., Storelvmo, T., Wang, H., and Watanabe, S.: The Geoengineering Model Intercomparison Project Phase 6 (GeoMIP6): Simulation design and preliminary results, Geosci. Model Dev., 8, 3379-3392, doi:10.5194/gmd-8-3379-2015, 2015.

Latham, J.: Control of global warming?, Nature, 347, 339–340, 1990.

Lau, W. K.-M., Wu, H.-T. and Kim, K.-M.: A canonical response of precipitation characteristics to global warming from CMIP5 models, Geophys. Res. Lett., 40, 3163–3169, doi:10.1002/grl.50420, 2013.

Lohmann, U., and Feichter, J.: Global indirect aerosol effects: A review, Atmos. Chem. Phys., 5, 715–737, doi:10.5194/acp-5-715- 2005, 2005.

Mautner, M.: Deep-space solar screens against climatic warming: technical and research requirements, in: Space Utilization and Applications in the Pacific, Proceedings of the Third Pacific Basin International Symposium on Advances in Space Science, Technology and Applications, American Astronautical Society, Los Angeles, 711, 1989.

Meinshausen, M., Smith, S. J., Calvin, K. et al. The RCP greenhouse gas concentrations and their extensions from 1765 to 2300, Climatic Change, 109:213, doi:10.1007/s10584-011-0156-z, 2011.

Moore, J. C., Rinke, A., Yu, X., Ji, D., Cui, X., Li, Y., Alterskjær, K., Kristjánsson, J. E., Muri, H., Boucher, O., Huneeus, N., Kravitz, B., Robock, A., Niemeier, U., Schulz, M., Tilmes, S., Watanabe, S., Yang, S.: Arctic sea ice and atmospheric circulation under the GeoMIP G1 scenario, J. Geophys. Res. -Atmos., 119, 567–583, doi:10.1002/2013JD021060, 2014.

Moore, J. C., Grinsted, A., Guo, X., Yu, X., Jevrejeva, S., Rinke, A., Cui, X., Kravitz, B., Lenton, A., Watanabe, S., and Ji, D.: Atlantic hurricane surge response to geoengineering. Proceedings of the National Academy of Sciences, PNAS, 112, 13794-13799, doi:10.1073/pnas.1510530112, 2015.

Niemeier, U., Schmidt, H., Alterskjær, K., and Kristjánsson, J. E.: Solar irradiance reduction via climate engineering: Impact of different techniques on the energy balance and the hydrological cycle, J. Geophys. Res. Atmos., 118, 11905–11917, doi:10.1002/2013JD020445, 2013.

Niemeier, U. and Timmreck, C.: What is the limit of climate engineering by stratospheric injection of SO2? Atmos. Chem. Phys., 15, 9129 – 9141 doi:10.5194/acp-15-9129-2015, 2015.

Orlowsky, B., and Seneviratne, S. I.: Global changes in extreme events: regional and seasonal dimension, Clim. Change, 110, 669–696, doi:10.1007/s10584-011-0122-9, 2012.

Pall, P., Allen, M. R., and Stone, D. A.: Testing the Clausius–Clapeyron constraint on changes in extreme precipitation under CO2 warming, Climate Dyn., 28, 351–363, doi:10.1007/ s00382-006-0180-2, 2007.

Pierce, J. R., Weisenstein, D. K., Heckendorn, P., Peter, T., and Keith, D. W.: Efficient formation of stratospheric aerosol for climate engineering by emission of condensible vapor from aircraft, Geophys. Res. Lett., 37, L18805, doi:10.1029/2010GL043975, 2010.

Pitari, G., Aquila, V., Kravitz, B., Robock, A., Watanabe, S., Cionni, I., Luca, N. D., Genova, G. D., Mancini, E., and Tilmes, S.: Stratospheric ozone response to sulfate geoengineering: Results from the Geoengineering Model Intercomparison Project (GeoMIP), J. Geophys. Res.-Atmos., 119, 2629–2653, 2014.

Pithan, F. and Mauritsen, T.: Arctic amplification dominated by temperature feedbacks in contemporary climate models, Nature Geoscience, 7, 181-184, doi:10.1038/NGEO2071, 2014.

Phipps, S. J., Rotstayn, L. D., Gordon, H. B., Roberts, J. L., Hirst, A. C., and Budd, W. F.: The CSIRO Mk3L climate system model version 1.0 – Part 1: Description and evaluation, Geosci. Model Dev., 4, 483-509, doi:10.5194/gmd-4-483-2011, 2011.

Radinović, D., and Ćurić, M.: Criteria for heat and cold wave duration indexes, Theor. Appl. Climatol., 107, 505-510, doi:10.1007/s00704-011-0495-8, 2012.

Robock, A., Oman, L., and Stenchikov, G. L.: Regional climate responses to geoengineering with tropical and Arctic SO2 injections, J. Geophys. Res., 113, D16101, doi:10.1029/2008JD010050, 2008.

Sanderson, B., Tebaldi, C., and O'Neill, B.: What would it take to achieve the Paris temperature targets?, *Geophys. Res. Lett.*, 43, 7133–7142, doi:10.1002/2016GL069563, 2016.

Schmidt, H., Alterskjær, K., Bou Karam, D., Boucher, O., Jones, A., Kristjánsson, J. E., Niemeier, U., Schulz, M., Aaheim, A., Benduhn, F., Lawrence, M., and Timmreck, C.: Solar irradiance reduction to counteract radiative forcing from a quadrupling of CO2: climate responses simulated by four earth system models, Earth Syst. Dynam., 3, 63–78, doi:10.5194/esd-3-63-2012, 2012.

Seneviratne, S. I., Koster, R. D., Guo, Z., Dirmeyer, P. A., Kowalczyk, E., Lawrence, D., Liu, P., Mocko, D., Lu, C., Oleson, K. W., and Verseghy, D.: Soil moisture memory in AGCM simulations: Analysis of Global Land- Atmosphere Coupling Experiment (GLACE) data, J. Hydrometeor., 7, 1090–1112, doi:10.1175/JHM533.1, 2006.

Seneviratne, S. I., Nicholls, N., Easterling, D., Goodess, C. M., Kanae, S., Kossin, J., Luo, Y., Marengo, J., McInnes, K., Rahimi, M., Reichstein, M., Sorteberg, A., Vera, C., and Zhang, X.: Changes in climate extremes and their impacts on the natural physical environment. In: IPCC Special Report on Extremes, 109-230, 2012.

Sillmann, J., Kharin, V. V., Zhang, X., Zwiers, F. W., and Bronaugh, D.: Climate extremes indices in the CMIP5 multimodel ensemble: Part 1. Model evaluation in the present climate, J. Geophys. Res. -Atmos., 118, 1716–1733, doi:10.1002/jgrd.50203, 2013a.

Sillmann, J., Kharin, V. V., Zwiers, F. W., Zhang X., and Bronaugh, D.: Climate extremes indices in the CMIP5 multimodel ensemble: Part 2. Future climate projections, J. Geophys. Res. Atmos., 118, 2473–2493, doi:10.1002/jgrd.50188, 2013b.

Smyth, J. E., Russotto, R. D., and Storelvmo, T.: Thermodynamic and dynamic responses of the hydrological cycle to solar dimming, Atmos. Chem. Phys., 17, 6439-6453, doi:10.5194/acp-17-6439-2017, 2017.

Stocker, T. F., Qin, D., Plattner, G.-K., Tignor, M., Allen, M. K., Boschung, J., Nauels, A., Xia, Y., Bex, V., and Midgley, P. M.: IPCC, 2013: Climate Change 2013: The Physical Science Basis. Contribution of Working Group I to the Fifth Assessment Report of the Intergovernmental Panel on Climate Change, Cambridge University Press, Cambridge, United Kingdom and New York, NY, USA, 1535 pp., 2013.

Sutton, R. T., Dong, B. W., and Gregory, J. M.: Land/sea warming ratio in response to climate change: IPCC AR4 model results and comparison with observations, Geophys. Res. Lett., 34, L02701, doi:10.1002/wcc.147, 2007.

Taylor, K. E., Stouffer, R. J., and Meehl, G. A.: An Overview of CMIP5 and the Experiment Design, B. Am. Meteorol. Soc., 93, 485–498, doi:10.1175/BAMS-D-11-00094.1, 2012.

Tebaldi, C., Hayhoe, K., Arblaster, J. M., and Meehl, G. A.: Going to extremes: An intercomparison of model-simulated historical and future changes in extreme events, Clim. Change, 79, 185–211, doi:10.1007/s10584-006-9051-4, 2006.

Tilmes, S., Garcia, R. R., Kinnison, D. E., Gettelman, A., and Rasch, P. J.: Impact of geoengineered aerosols on the troposphere and stratosphere, J. Geophys. Res., 114, D12305, doi:10.1029/2008JD011420, 2009.

Tilmes, S., Fasullo, J., Lamarque, J.-F., Marsh, D. R., Mills, M., Alterskjaer, K., Muri, H., Kristjánsson, J. E., Boucher, O., Schulz, M., Cole, J. N. S., Curry, C. L., Jones, A., Haywood, J., Irvine, P. J., Ji, D., Moore, J. C., Karam, D. B., Kravitz, B., Rasch, P. J., Singh, B., Yoon, J.-H., Niemeier, U., Schmidt, H., Robock, A., Yang, S., and Watanabe, S.: The hydrological impact of geoengineering in the Geoengineering Model Intercomparison Project (GeoMIP), J. Geophys. Res. -Atmos., 118, 11,036–11,058, doi:10.1002/jgrd.50868, 2013.

Tilmes, S., Jahn, A., Kay, J. E., Holland, M., and Lamarque, J.-F.: Can regional climate engineering save the summer Arctic sea ice? Geophys. Res. Lett., 41, 880–885, doi:10.1002/2013GL058731, 2014.

Volodin, E. M., Kostrykin, S. V., and Ryaboshapko, A. G.: Climate response to aerosol injection at different stratospheric locations, Atmos. Sci. Let., 12, 381-385, doi:10.1002/asl.351, 2011.

Wang, Q., Moore, J. C., and Ji, D.: A statistical examination of the effects of stratospheric sulphate geoengineering on tropical storm genesis, Atmos. Chem. Phys. Discuss., doi:10.5194/acp-2018-142, in review, 2018.

Watanabe, S., Hajima, T., Sudo, K., Nagashima, T., Takemura, T., Okajima, H., Nozawa, T., Kawase, H., Abe, M., Yokohata, T., Ise, T., Sato, H., Kato, E., Takata, K., Emori, S., and Kawamiya, M.: MIROC-ESM 2010: model description and basic results of CMIP5-20c3m experiments, Geosci. Model Dev., 4, 845-872, doi:10.5194/gmd-4-845-2011, 2011.

Xia, L., Nowack, P. J., Tilmes, S., and Robock, A.: Impacts of stratospheric sulfate geoengineering on tropospheric ozone, Atmos. Chem. Phys., 17, 11913-11928, doi:10.5194/acp-17-11913-2017, 2017.

Yu, X., Moore, J. C., Cui, X., Rinke, A., Ji, D., Kravitz, B., and Yoon, J.-H.: Impacts, effectiveness and regional inequalities of the GeoMIP G1 to G4 solar radiation management scenarios, Global Planet Change, 129, 10-22, doi:10.1016/j.gloplacha.2015.02.010, 2015.

Zhang, X., Alexander, L., Hegerl, G. C., Jones, P., Tank, A. K., Peterson, T. C., Trewin, B., and Zwiers, F. W.: Indices for monitoring changes in extremes based on daily temperature and precipitation data, WIREs Clim. Change, 2, 851–870, doi:10.1002/wcc.147, 2011.

Table 1: GeoMIP Models used in this study

No.	Model	Institution	Resolution (Lon×Lat Level)
1	BNU−ESM (Ji et al. 2014)	Beijing Normal University, China	2.8°×2.8° L26
2	CanESM2 (Arora et al., 2011)	Canadian Centre for Climate Modelling, Canada	2.8°×2.8° L35
3	GISS-E2-R (Schmidt et al. 2011)	Goddard Institute for Space Studies, USA	2.5°×2.0° L40
4	HadGEM2−ES (Collins et al. 2011)	Met Office Hadley Centre, UK	1.875°×1.25° L40
5	MIROC−ESM (Watanabe et al. 2011)	AORI, NIES, JAMSTEC, Japan	2.8°×2.8° L80
6	NorESM1-M (Bentsen et al. 2013)	University of Oslo, Norway	1.9°x2.5° L26

Table 2: Indices of climate extremes

Index	Description	Definition	Units
TNn	Coldest daily Tmin	Annual minimum value of daily minimum temperature	℃
TXx	Warmest daily Tmax	Annual maximum value of daily maximum temperature	℃
Rx5day	Wettest consecutive five days	Maximum of consecutive 5-day (cumulative) precipitation amount	mm
CSDI	Cold spell duration	Number of consecutive days (> 6 days) when daily minimum temperature falls below the 10th percentile of piControl	days
WSDI	Warm spell duration	Number of consecutive days (> 6 days) when daily maximum temperature falls above the 90th percentile of piControl	days
CDD	Consecutive dry days	Maximum number of consecutive days when precipitation < 1 mm	days

Table 3: Differences and ratios in means and climate extreme indices over the 40-year analysis period.

Experiments	Indices	Land	Ocean	Global
$G1 - abrupt4 \times CO2$	TNn(°C)	-6.4	-4.5	-5.1
	TXx(°C)	-6.2	-3.7	-4.4
	Rx5day(mm)	-12.3	-13.4	-13.1
	TOA net radiation flux(Wm^{-2})	-1.6	-3.2	-2.8
	Mean T(°C)	-5.6	-3.7	-4.3
	Mean P(mm a^{-1})	-81.0	-106.4	-98.9
$G4 - rcp45$	TNn(°C)	-0.9	-0.6	-0.7
	TXx(°C)	-0.8	-0.5	-0.6
	Rx5day(mm)	-1.6	-1.9	-1.8
	TOA net radiation flux(Wm^{-2})	-0.2	-0.4	-0.4
	Mean T(°C)	-0.7	-0.5	-0.5
	Mean P(mm a^{-1})	-8.2	-16.6	-14.1
$\frac{G1 - abrupt4 \times CO2}{G4 - rcp45}$	TNn(°C)	6.9	7.6	7.3
	TXx(°C)	7.5	7.7	7.6
	Rx5day(mm)	7.8	7.2	7.3
	TOA net radiation flux(Wm^{-2})	8.3	7.6	7.7
	Mean T(°C)	7.9	8.3	8.1
	Mean P(mm a^{-1})	9.8	6.4	7.0